МІНІСТЕРСТВО ОСВІТИ І НАУКИ УКРАЇНИ

НАЦІОНАЛЬНИЙ АВІАЦІЙНИЙ УНІВЕРСИТЕТ

КАФЕДРА КОНСТРУКЦІЇ ЛІТАЛЬНИХ АПАРАТІВ

ДОПУСТИТИ ДО ЗАХИСТУ
Завідувач кафедри
д.т.н., професор
_____Сергій ІГНАТОВИЧ
«___ »_____2022 р.

КВАЛІФІКАЦІЙНА РОБОТА
ВИПУСКНИКА ОСВІТНЬОГО СТУПЕНЯ МАГІСТРА
ЗІ СПЕЦІАЛЬНОСТІ
«АВІАЦІЙНА ТА РАКЕТНО-КОСМІЧНА ТЕХНІКА»

Тема: «Дослідження нелінійної поведінки властивостей матеріалів при циклічних навантаженнях»

Виконавець: _____ **Вейцюнь Чень**

Керівник: к.т.н., доцент _____ **Святослав ЮЦКЕВИЧ**

Охорона праці: к.т.н., доцент _____ **Катерина КАЖАН**

Охорона навколишнього середовища:
к.т.н., професор _____ **Леся ПАВЛЮХ**

Нормоконтролер: к.т.н., доцент _____ **Володимир КРАСНОПОЛЬСЬКИЙ**

Київ 2022

MINISTRY OF EDUCATION AND SCIENCE OF UKRAINE

NATIONAL AVIATION UNIVERSITY

DEPARTMENT OF AIRCRAFT DESIGN

PERMISSION TO DEFEND
Head of the department,
Dr. of Sc., professor
_____ Sergiy IGNATOVYCH
"___" _____ 2022

MASTER DEGREE THESIS

ON SPECIALITY

”AVIATION AND ROCKET-SPACE TECHNOLOGIES”

Topic: «Investigation of nonlinear behaviour of materials properties during cycling loads»

Fulfilled by: _____ **Weiqun Chen**

Supervisor:

Ph.D, associate professor _____ **Sviatoslav YUTSKEVYCH**

Labor protection advisor:

Ph.D, associate professor _____ **Katerina KAZHAN**

Environmental protection adviser:

Ph.D, professor _____ **Lesya PAVLYUKH**

Standards inspector:
PhD, associate professor _____ **Volodymyr KRASNOPOLSKYI**

Kyiv 2022

НАЦІОНАЛЬНИЙ АВІАЦІЙНИЙ УНІВЕРСИТЕТ

Факультет аерокосмічний

Кафедра конструкції літальних апаратів

Освітній ступінь «Магістр»

Спеціальність 134 «Авіаційна та ракетно-космічна техніка»

Освітньо-професійна програма «Обладнання повітряних суден»

ЗАТВЕРДЖУЮ
Завідувач кафедри
д.т.н., професор
_____Сергій ІГНАТОВИЧ
«___» _____2022 р.

ЗАВДАННЯ

на виконання кваліфікаційної роботи пошукача

Вейцюнь Чень

1. Тема роботи «Дослідження нелінійної поведінки властивостей матеріалів при циклічних навантаженнях», затверджена наказом ректора від 05 жовтня 2022 року №1861/ст.

2. Термін виконання проекту: з 06 жовтня 2022р. по 30 Листопад 2022 р.

3. Вихідні дані до проекту: Параметри D16T, Геометрична форма і розміри зразка та основні параметри спектру навантаження TWIST.

4. Зміст пояснювальної записки: Існуючі дослідження нелінійної поведінки матеріалів при циклічних навантаженнях, експериментальна методика та випробувальні машини для випробувань на втому та мікротвердість, експериментальні результати випробувань на мікротвердість, охорона праці та навколишнього середовища.

5. Перелік обов’язкового графічного (ілюстративного) матеріалу: презентація Power Point, малюнки та схеми.

6. Календарний план-графік

№ пор.	Завдання	Термін виконання	Відмітка про виконання
1	Дослідницька література про нелінійну поведінку матеріалів під циклічним навантаженням.	06.10.2022–18.10.2022	
2	Аналіз лінійних методів для прогнозування залишкової довговічності матеріалів.	19.10.2022-29.10.2022	
3	Аналіз нелінійних методів для прогнозування залишкової довговічності матеріалів.	30.10.2022-07.11.2022	
4	Випробування на втому та мікротвердість, аналіз результатів випробувань.	06.10.2022-31.10.2022	
5	Виконання розділів, присвячених охороні навколишнього середовища та праці.	01.11.2022-04.11.2022	
6	Оформлення дипломної роботи	05.11.2022-10.11.2022	

7. Консультанти з окремих розділів

Розділ	Консультанти	Дата, підпис	
		Завдання видав	Завдання прийняв
Охорона праці	Катерина КАЖАН		
Охорона навколишнього середовища	Lesya PAVLYUKH		

8. Дата видачі завдання: 5 жовтня 2022 р.

Керівник кваліфікаційної роботи: _____ Святослав ЮЦКЕВИЧ

Завдання прийняв до виконання: _____ Вейцюнь Чень

NATIONAL AVIATION UNIVERSITY

Aerospace faculty

Department of aircraft design

Educational Degree «Master»

Specialty 134 «Aviation and Rocket-Space Technologies»

Educational professional program «Aircraft equipment»

APPROVED BY

Head of Department,

Dr. of Sc., professor

_____ Sergiy IGNATOVYCH

"___" _____ 2022

TASK

For the master degree thesis

Weiqun Chen

1. Topic: «Investigation of nonlinear behaviour of materials properties during cycling loads», approved by the Rector's order № 1861 «05» October 2022 year.
2. Period of work execution: from 05 October 2022 year to 30 November 2022 year.
3. Initial data: Parameters of D16T, Geometrical shape and dimensions of specimen and main parameters of TWIST loading spectrum.
4. Content: Existing researches on nonlinear behaviour of materials under cycling loads, experimental procedure and test machines for fatigue testings and microhardness testings, experimental results of microhardness testings, labor and environmental protection.
5. Required material:power point presentation, drawings and diagrams

6.Thesis schedule:

№	Task	Time limits	Done
1	Research literature on nonlinear behaviour of materials under cycling load.	06.10.2022–18.10.2022	
2	Analysis the linear methods to predict the residual fatigue life of materials.	19.10.2022-29.10.2022	
3	Analysis the nonlinear methods to predict the residual fatigue life of materials.	30.10.2022-07.11.2022	
4	Carry out fatigue testings and microhardness testings, and analysis the testing results.	06.10.2022-31.10.2022	
5	Implementation of the parts, devoted to environmental and labor protection.	01.11.2022-04.11.2022	
6	Edit and correct the draft, modify the format.	05.11.2022-10.11.2022	

7. Special chapter advisers

Chapter	Consultants	Date, signature	
		Task Issued	Task Received
Labor protection	PhD, associate professor Katerina KAZHAN		
Environmental protection	PhD, professor Lesya PAVLYUKH		

8. Date: 05 October 2022 year.

Supervisor: _____ Sviatoslav YUTSKEVYCH

Student: _____ Weiqun Chen

РЕФЕРАТ

Пояснювальна записка дипломної роботи магістра "Дослідження нелінійної поведінки властивостей матеріалів при циклічних навантаженнях"

78 с., 37 рис., 13 табл., 38 джерел

Об'єктом дослідження є нелінійна поведінка властивостей матеріалів.

Предметом дослідження є аналіз нелінійної поведінки властивостей матеріалу при циклічному навантажувані для прогнозування залишкової довговічності.

Метою магістерської роботи є прогнозування залишкової втомної довговічності матеріалів методом мікротвердості.

Методи дослідження та розробки полягають у аналізі існуючих дослідницьких робіт з використання неруйнівних методів для дослідження нелінійної поведінки властивостей матеріалів під час циклічних навантажень, аналізу зв’язку нелінійної поведінки властивостей матеріалів із залишковою довговічністю, а потім проведення деяких експериментів, щоб підтвердити це.

У дисертації аналізуються наявні науково-дослідні роботи з використання неруйнівних методів для прогнозування залишкової довговічності, методика експерименту та випробувальні машини для випробувань на втому та мікротвердість, а також результат контролю мікротвердості.

Практична цінність роботи доведена тим, що вимірювання мікротвердості є простим і ефективним способом прогнозування залишкової довговічності. Коли має місце складна нелінійна поведінка, використання двох або більше методів НК може зробити більш точним прогнозування терміну служби втомленості.

Матеріали магістерського диплому можуть бути використані в авіаційній промисловості та в навчальному процесі, пов'язаному з нелінійною поведінкою властивостей матеріалів при циклічних навантаженнях та прогнозуванням втомної довговічності.

ЛІТАК, ВТОМА, НЕЛІНІЙНА ПОВЕДІНКА, НЕРУЙНЮВАЛЬНИЙ ВИПРОБУВАННЯ, ВИПРОБУВАННЯ НА МІКРОТВЕРДІСТЬ

ABSTRACT

Master degree thesis “Investigation of nonlinear behaviour of materials properties during cycling loads”

78 pages, 37 figures, 13 table, 38 references

Object of study is the nonlinear behaviour of materials properties.

Subject of study is analyzing nonlinear behavior of material properties under cycling to predict residual fatigue life.

Aim of master degree thesis is to predict residual fatigue life of materials by using microhardness testing method.

Research and development methods are analyzing the existing research works on using nondestructive methods to investigate nonlinear behaviour of materials properties during cycling loads, analysis the relationship of nonlinear behaviour of materials properties with the residual fatigue life, then do some experiments to prove it.

The thesis consists analysis existing research works on using nondestructive methods to predict the residual fatigue life, experimental procedure and test machines of fatigue testing and microhardness testing, and the result of microhardness testing.

Practical value of the work is proved that the microhardness testing is a easy and effective way to be used to predict the residual fatigue life. And When complex nonlinear behavior occurs, the use of two or more NDT techniques can make fatigue life prediction more accurate.

The materials of the master's diploma can be used in the aviation industry and in the educational process related to nonlinear behaviour of materials properties during cycling loads and fatigue life prediction.

AIRCRAFT, FATIGUE, NONLINEAR BEHAVIOUR, NONDESTRUCTIVE TESTING, MICROHARDNESS TESTING

CONTENT

ABBREVIATIONS

NDT – Nondestructive testing

CA – Constant amplitude

VA – Variable amplitude

XRD – X-ray diffraction

FWHM – Full width at half maximum

SHM – structural health monitoring

AE – Acoustic emission

SLH – Standardized load-time histories

OSH – Occupational safety and health

ILO – International Labor Organization

ICAO – International Civil Aviation Organization

SARPs – Standards and Recommended Practices

CORSIA – Carbon Offsetting and Reduction Scheme for International Aviation

INTRODUCTION

Fatigue failure is a common failure mode in all aircraft metals and alloys. Due to repeated takeoffs and landings, even during cruise, the metals and alloys on the aircraft can weaken and eventually fail due to repeated cyclic loading.

This weakening behavior is manifested by the appearance of cracks. The cracks are initially microscopic, however, with continued use of the aircraft, the cracks will expand and eventually become visible. The effects of fatigue on the plane occur almost immediately when the plane flies for the first time. Aging becomes a very serious problem when aircraft are subject to cumulative flight and cannot be effectively maintained. Statistics show that most of the reasons for the failure of aircraft components are caused by fatigue, accounting for about 60% of all failures [1].

Fatigue studies of materials are necessary to understand material failure mechanisms and predict residual fatigue life. The process of fatigue failure is generally considered to be the initiation of microcracks from the surface of the material and propagation with the help of cyclic loading, ultimately leading to the fracture of metals and alloys.

Although fatigue is gradual, fracture occurs when the stress exceeds the fracture stress. The serious consequence of material failure is the destruction of the aircraft. In order to understand the damage and predict fatigue life of parts composed of metals or metal alloys under cyclic loading, it is crucial to understand the microstructural mechanisms of cyclic plastic deformation. By studying the relationship between material properties and cyclic loading, it may be possible to predict the amount of damage and residual fatigue life of materials, such as changes in microhardness and electrical resistance under cyclic loading.

It was found that non destructive testing (NDT) is the best way to understand damage and predict the remaining fatigue life of a part. Under the condition that the object is not damaged, the changes in physical quantities such as heat, sound, light, electricity, and magnetism caused by abnormal internal structure or defects of the material are used to detect the internal and surface defects of various materials, parts or structures, and predict residual fatigue life.

The existing NDTs used to detect fatigue cracks and predict the residual fatigue life have: micro hardness testing, X-ray diffraction, electrical resistance testing, acoustic emission, etc [6-19].

These methods utilize principles and technologies such as X-ray, ultrasonic, microhardness, and electromagnetism to detect defects, chemical and physical parameters of materials and parts without affecting the function or current working state of the test object. These techniques provide reliable solutions for studying fatigue damage and fatigue life prediction of materials.

This work analyzed the relevant researches on predicting the fatigue damage degree and residual fatigue life of materials by using nondestructive testing technology, briefly explains their research process and results, and gives the most applicable and effective fatigue damage degree and residual fatigue life. Finally, it is found that the microhardness testing technology is a simple and effective method to predict the residual fatigue life of materials, and the experiment of predicting the residual fatigue life by microhardness is carried out. At the same time, it is proposed that when the nonlinear behavior of materials under fatigue load is complex, the use of various non-destructive testing techniques can improve the accuracy of fatigue life prediction.

1. STATE OF THE ART LITERATURE REVIEW

1.1. Linear method of fatigue life prediction

When people realized the influence of fatigue on material properties, people start to think about how to determine a boundary stage of material fatigue damage and residual life. The simplest method for fatigue life predictions was linear description of material fatigue behavior that was used by Miner [2]. In 1945, M.A. Miner popularized a rule that had first been proposed by A.Palmgren in 1924. As shown in the figure 1.1. This rule, also known as Miner's rule or Palmgren-Miner linear damage hypothesis(formula 1), states that where there are k different stress magnitudes in a load spectrum, S_i ($1 \leq i \leq k$), each contributing $n_i(S_i)$ cycles, then if $N_i(S_i)$ is the number of cycles to failure of a constant stress reversal S_i, failure occurs when:

$$\sum_{i=1}^{k} \frac{n_i \times S_i}{N_i \times S_i} = 1 \qquad (1)$$

The constant is experimentally found to be between 0.7 and 2.2. Usually for design purposes, constant is assumed to be 1.

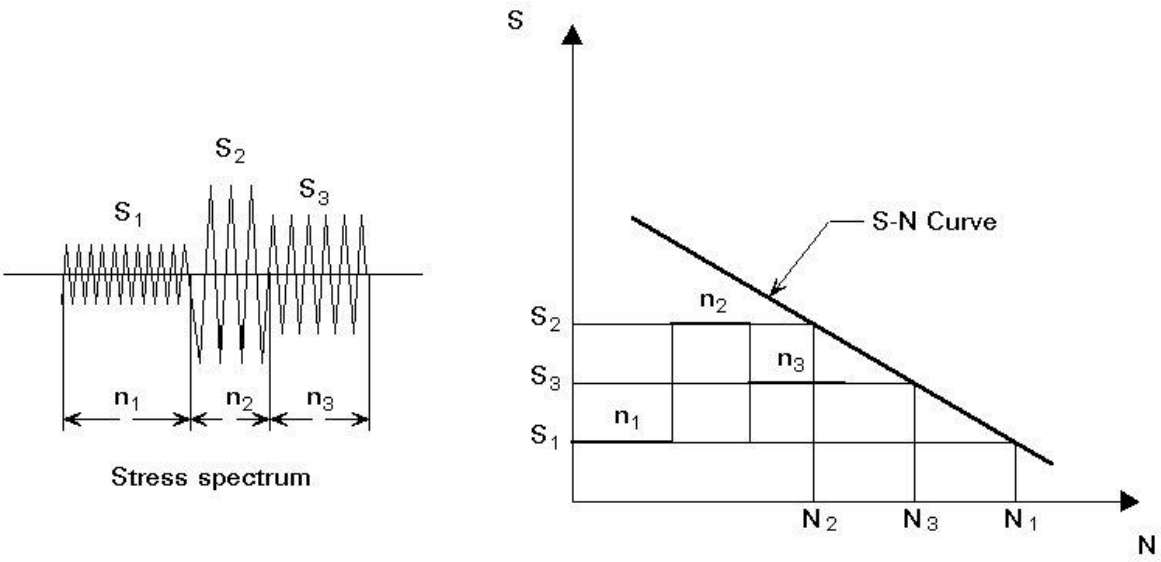

Figure 1.1 - Scheme for linear Miner law [2].

Miner's rule states that the first stress cycle is as destructive as the last stress cycle at the same stress level. Miner's rule assumes that the fatigue life consumed by stress cycles is proportional to the total number of cycles in the fatigue life, if this is the only stress level applied to the part. For example, if a part fails after 1000 cycles at a certain stress level, then 50 cycles at the same stress level will consume 5% of the fatigue life. Repeated stress at another stress level will consume another method of similarly calculated fatigue life portion. When 100% of the fatigue life is consumed in this way, the part fails [2].

Unfortunately, this rule is not reliable, because of some elementary shortcomings. Three important deficiencies are [3]:

(i) The experimental data used to plot the SN curves are scattered and not linear as in theory;

(ii) Miner's rule states that cycles with stress amplitudes below the fatigue limit will not cause damage to the material. In practice, however, these cycles with stress amplitudes below the fatigue limit may amplify fatigue damage caused by cycles with amplitudes above the fatigue limit;

(iii) Components are prone to stress concentrations at the notch, and these stresses form residual stresses at the root of the notch. The Miner's Law ignores the residual stress effect at the notch, which affects the fatigue damage contribution of subsequent cycles.

1.2. Nonlinear methods of fatigue life prediction

When it became apparent that Miner's rule could not lead to a reliable prediction of fatigue damage accumulation and fatigue life, other alternative nonlinear fatigue life prediction methods were proposed:

(i) A non-linear damage function

Figure 1.2a shows that, according to Miner's rule, the fatigue damage during CA loading increases linearly with the number of loading cycles. Figure 1.2b shows a modification of Miner's rule, where the fatigue damage during loading increases non-linearly with the number of loading cycles. It is easy to show that a nonlinear damage function like Figure 1.2b still obeys Miner's rule [4].

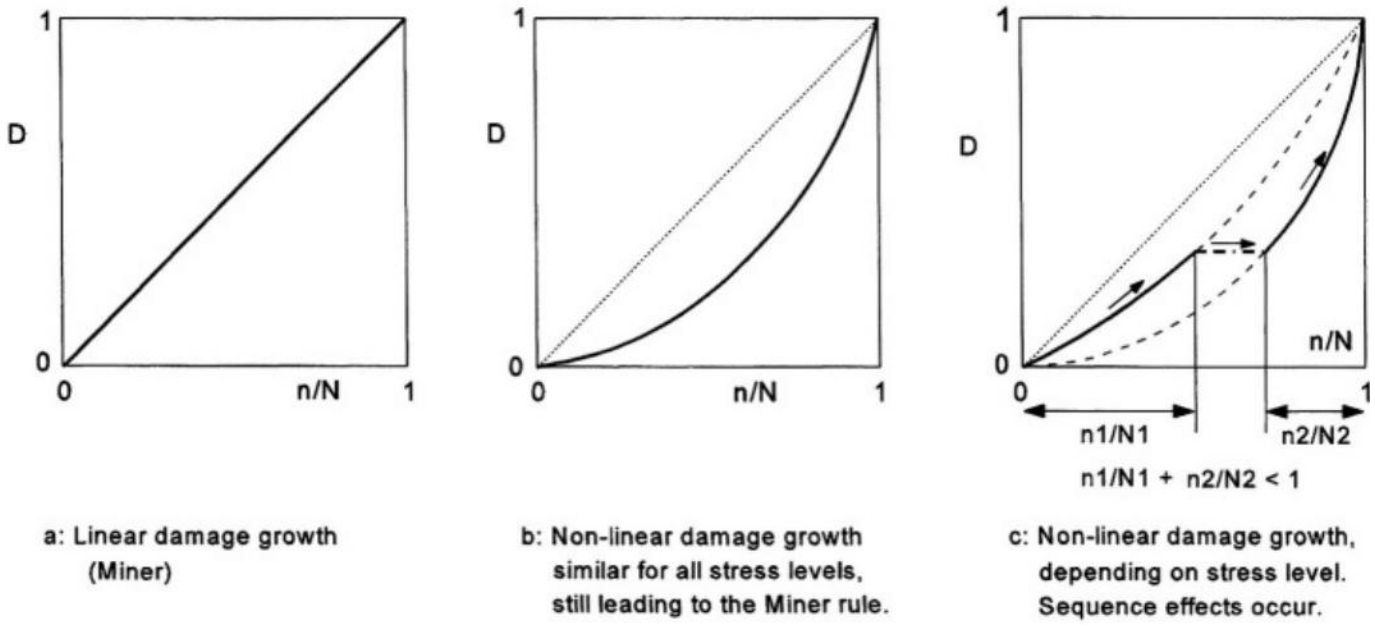

Figure 1.2 - Fatigue damage characterized by a single damage parameter: a - Linear damage growth; b - Non linear damage growth similar for all stress level, still leading to the Miner rule; c - Non linear damage growth, depending on stress level, sequence effects occur [3].

Figure 1.2c shows a simple variable amplitude (VA) test consisting of two constant amplitude (CA) cycles. During the first block, the damage increases along the first curve, during the second block it transitions to another damage curve and then increases along the second curve until failure at D=1. The sum of the two curves n/N is clearly less than 1. However, reversing the order of the two loop blocks would result in the sum of the two n/N contributions being greater than 1.

(ii) Damage calculations with extrapolation of S-N curves below the fatigue limit.

To improvement the essential shortcoming of Miner rule that cycles with a stress amplitude below the fatigue limit are supposed to be non-damaging, an extrapolation curve B was proposed in the Figure 1.3. Line H in Figure 1.3 is an other suggestion for extending the S-N curves below the fatigue limit was proposed by Haibach [5].

Calculated fatigue life based on the S-N curves A and B for both spectra H1 and H2 are shown in Table 1.1. The results show that fatigue life is shorter if the Miner prediction is based on the extrapolated curve B. Due to this result, B/A of spectrum H2 in Table 1 is

much smaller than spectrum H1. Because spectrum H2 has relatively more cycles below the fatigue limit.

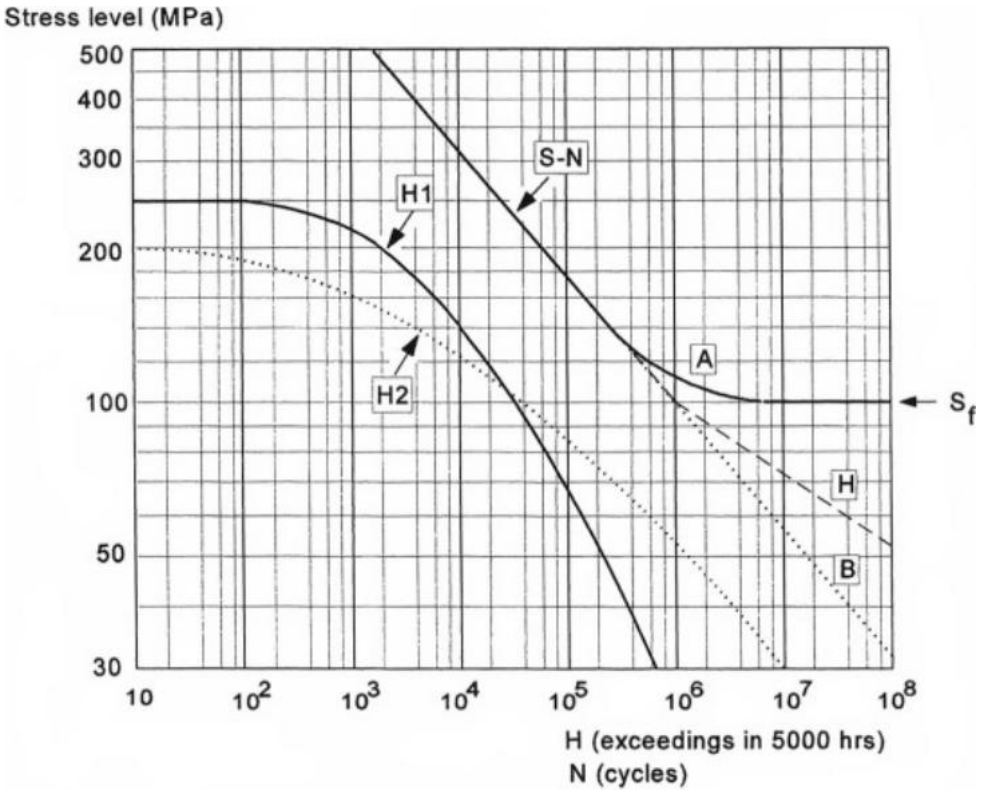

Figure 1.3 - Two load spectra and an S-N curve used in a Miner calculation [3].

The extrapolation S-N curve B shows that an additional safety margin for fatigue life prediction is introduced [3].

Table 1.1 - Miner prediction by using different S-N curve A and B for Spectrum H1 and H2 [3].

S-N curve used	Fatigue life(hrs)		Life ratio(H1/H2)
	Spectrum H1	Spectrum H1	
A	37000	66000	0.56
B	23000	7000	3.3
	B/A=0.62	B/A=0.11	

(iii) The relative Miner rule

Schütz proposed an non-conservative predictions of the Miner-rule. He replaced Miner-rule $\Sigma n/N=1$ by "relative Miner-rule" $\Sigma n/N=q$, $q<1$. q was chosen based on the results of a VA test with historical loading times similar to the problem studied.

Relative Miner's rule can also be interpreted as using Miner's rule with a safety factor to explain possible non-conservative life predictions[3].

(iv) The strain history prediction model

When realizing that the notch root easily introduces local residual stress and affects the fatigue damage contribution of subsequent cycles. Knowing the true strain history at the root of the notch becomes a viable solution to this problem. At the same time, it is also possible to predict the fatigue life of VA loads by predicting the strain history at the root of the notch (Figure 1.4 and Figure 1.5).

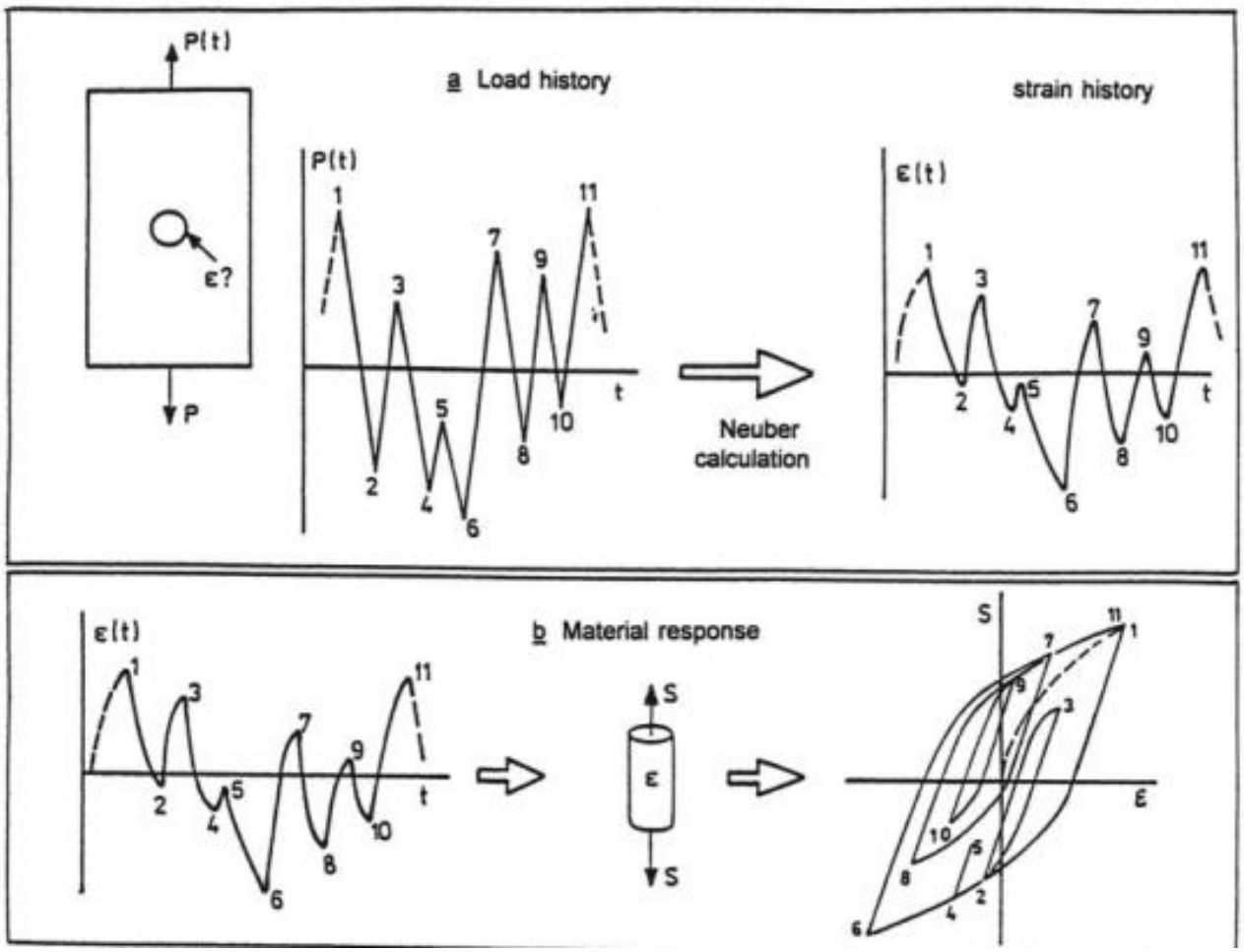

Figure 1.4 - The notch-root strain history (a) and material response (b) [3].

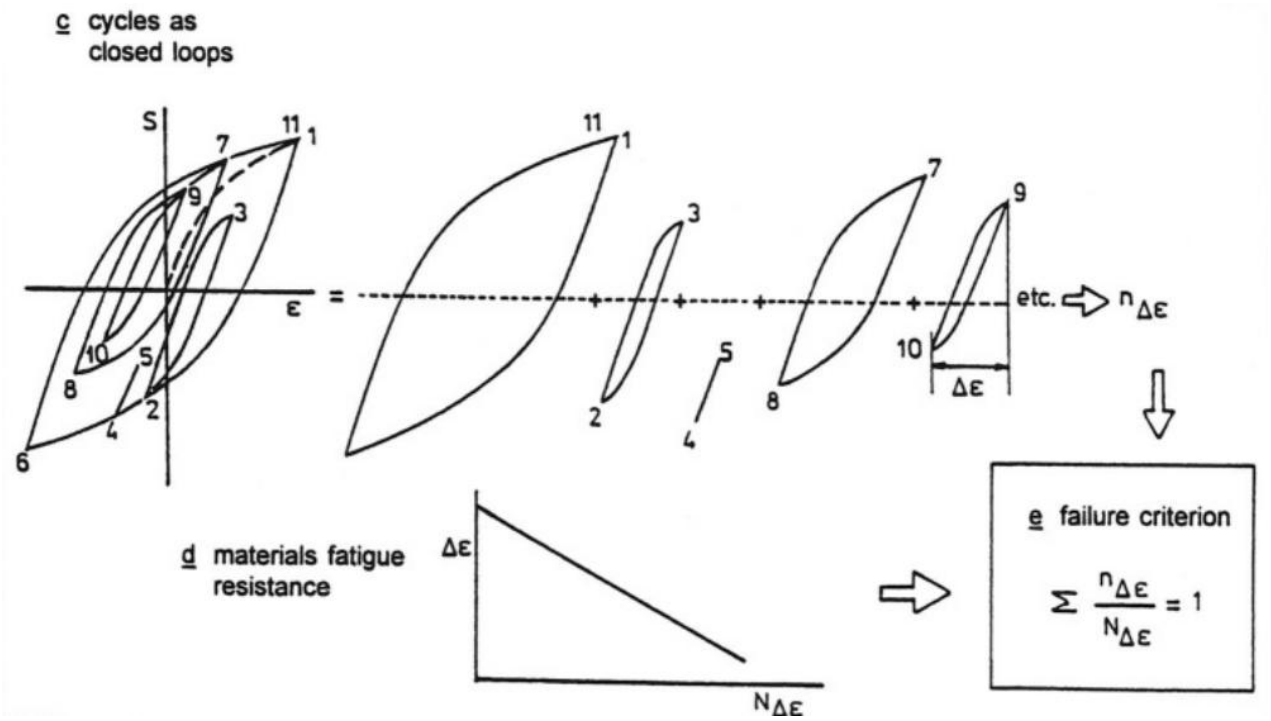

Figure 1.5 - Principles of the notch-root strain based prediction model. (c) cycles as closed loops, (d) materials fatigue resistance, (e) failure criterion [3].

(v) Predictions based on crack growth from an equivalent initial flaw

Crack growth prediction methods based on equivalent initial defects show that fatigue life prediction can be done by predicting crack growth if the crack growth covers the entire fatigue life. At present, the equivalent initial defect method has been used to predict the fatigue life of aluminum alloys [3].

1.3. Non destructive testing used to investigate the fatigue behavior of material

In addition, when non-destructive testing technology was developed, it was widely used in crack detection and fatigue life prediction because it could detect defects, chemical and physical parameters using rays, ultrasound, infrared, electromagnetic, etc. without destroying the properties of materials.

The following it was introduced the several types of non-destructive testing technologies, which are used for fatigue damage and fatigue life prediction of materials.

1.3.1. X-ray diffraction

In the process of material fatigue, it is mainly the microstructure of the material surface area that changes, and X-ray diffraction technology can penetrate the area of about 5-10mm on the material surface, so X-ray diffraction technology is suitable for material fatigue detection.

Studies have shown that the shape and location of XRD peaks depend on micro structural parameters such as grain size, residual stress, micro deformation, stacking faults, etc[6]. So the XRD technique is used to evaluate micro deformations. And it was known that micro-deformations are evaluated from the full width at half maximum (FWHM) of the diffraction peak and residual stresses are estimated from the peak shift [7].

Experimental procedures: The fatigue test and x-ray diffraction measurement are performed at the same time. The material parameters detected by the X-ray diffraction were peak intensity (peak height) and full width at half maximum (FWHM). Fatigue testing is periodically interrupted for XRD measurements at intervals of 10,000 load cycles until final failure.And the test machines are shown in the Figure 1.6.

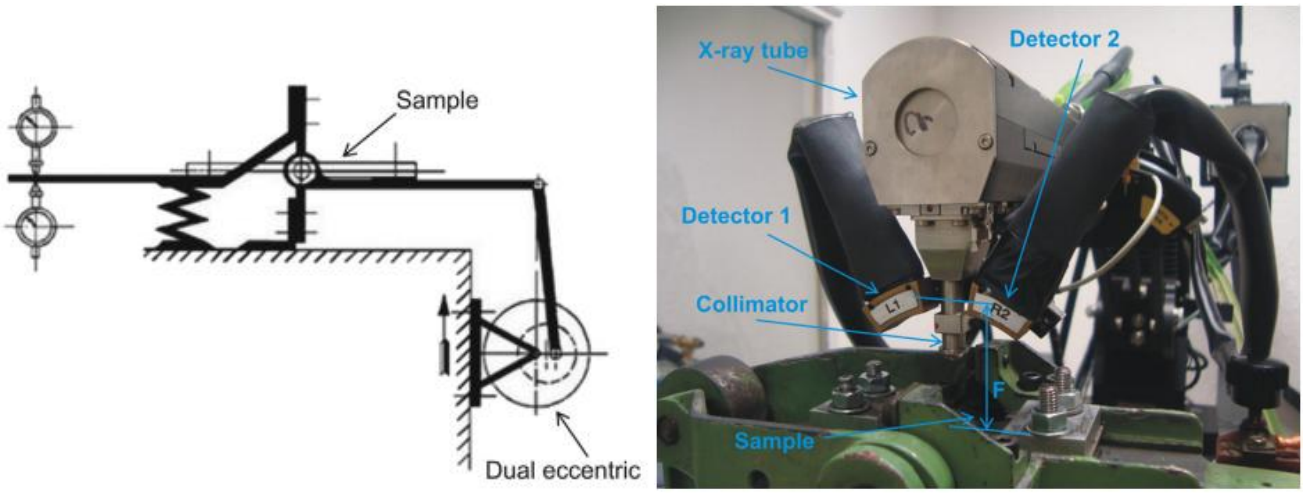

Figure 1.6 - Bending fatigue test machine and X-ray diffraction measurements [7].

Experimental results:

(i) As-machined API 5L X60 grade steel

Table 1.2 - Main parameters of as-machined specimens [7].

Specimen	Strain amplitude	Stress amplitude (MPa)		R	N (cycles)
T1EF04	0.17%	319	$0.61\sigma_0$	-1.1	147,300
T1EF05					106,600
T1EF08					143,200
T1EF15					191,100
T1EF22	0.19%	361	$0.69\sigma_0$	-1	63,600
T1EF24					48,100

The change in FWHM measured at a given number of cycles is given by FWHM-$FWHM_0$, where $FWHM_0$ is the value of FWHM at N=0. The main parameters of as-machined specimens are shown in the table 1.2. And according to the figure 1.7, three stages can be identified in the evolution of FWHM with cycling.

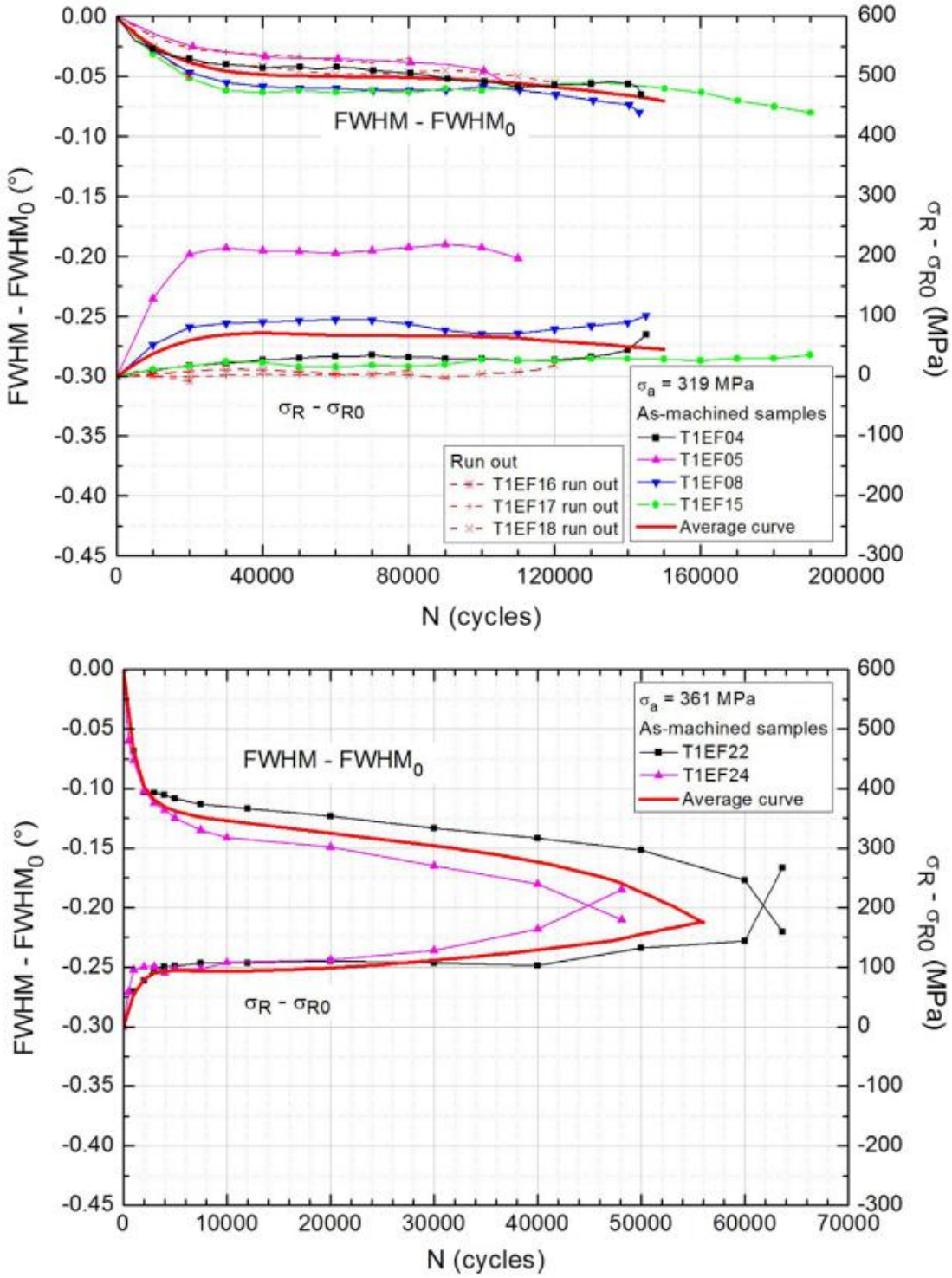

Figure 1.7 - Changes in FWHM and residual stresses with cycling of as-machined specimens at σ_a=319 and 361MPa (R = −1) [7].

The first stage occurs in the early stage of fatigue, and the value of FWHM decreases rapidly. In the second stage, the decreasing speed of FWHM decreases, even in a constant state. The duration of this phase is approximately 50% of the fatigue life. Finally, the value of the FWHM in the third stage continues to decrease until the end of the fatigue life. [7].

In stage 1, the decrease in FWHM may be related to the movement of dislocations, the rearrangement of initial dislocations, and the reduction of microdeformation. In the stage 2, the decreasing rate of FWHM decreases, which may be related to the microcracks and the first stage crack propagation. In stage 3, the reduction in FWHM may be related to the coalescence of micro-cracks and the formation of macro-cracks and the resulting stress relaxation, which then propagate to eventual failure.

Figure 1.8 shows the average curve of the FWHM change during fatigue testing at four different alternating stress amplitudes. An increase in stress amplitude was found to increase the change in FWHM and shorten the duration of each phase.

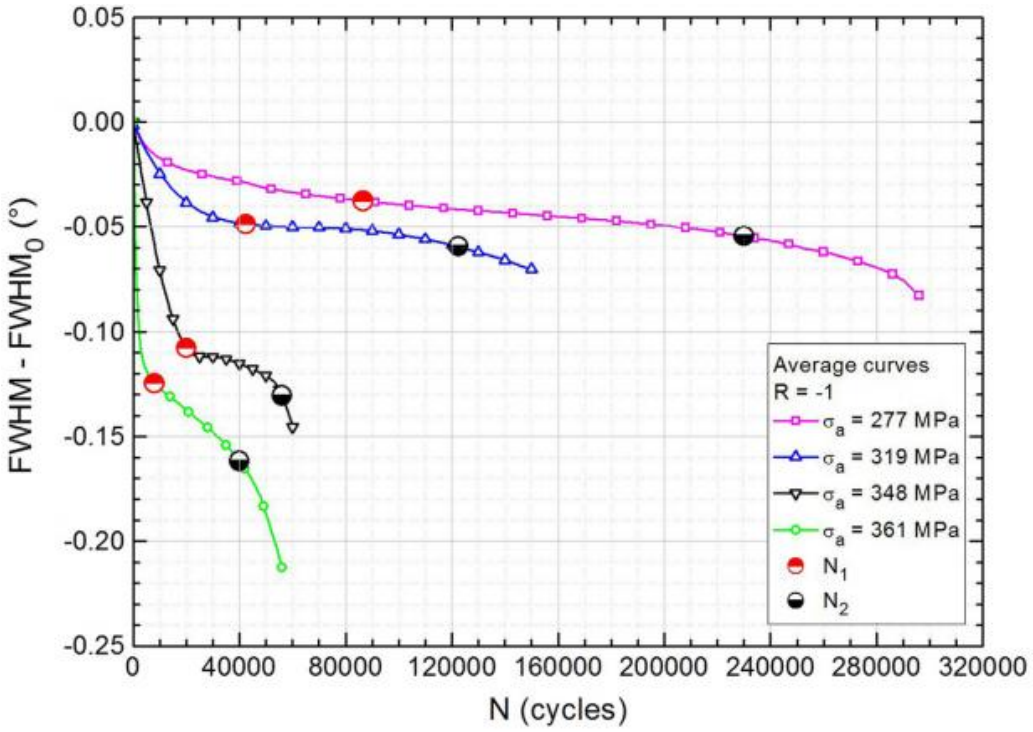

Figure 1.8- Average curves of changes in FWHM with cycling of as-machined specimens at different stress amplitudes. The numbers of cycles at the end of stages 1 and 2 are defined as N_1 and N_2 [7].

(ii) Annealed API 5L X60 grade steel

As in the case of machined specimens, the evolution of FWHM during fatigue testing of annealed specimens also presents three stages. As shown in the figure 1.9 and table 1.3.

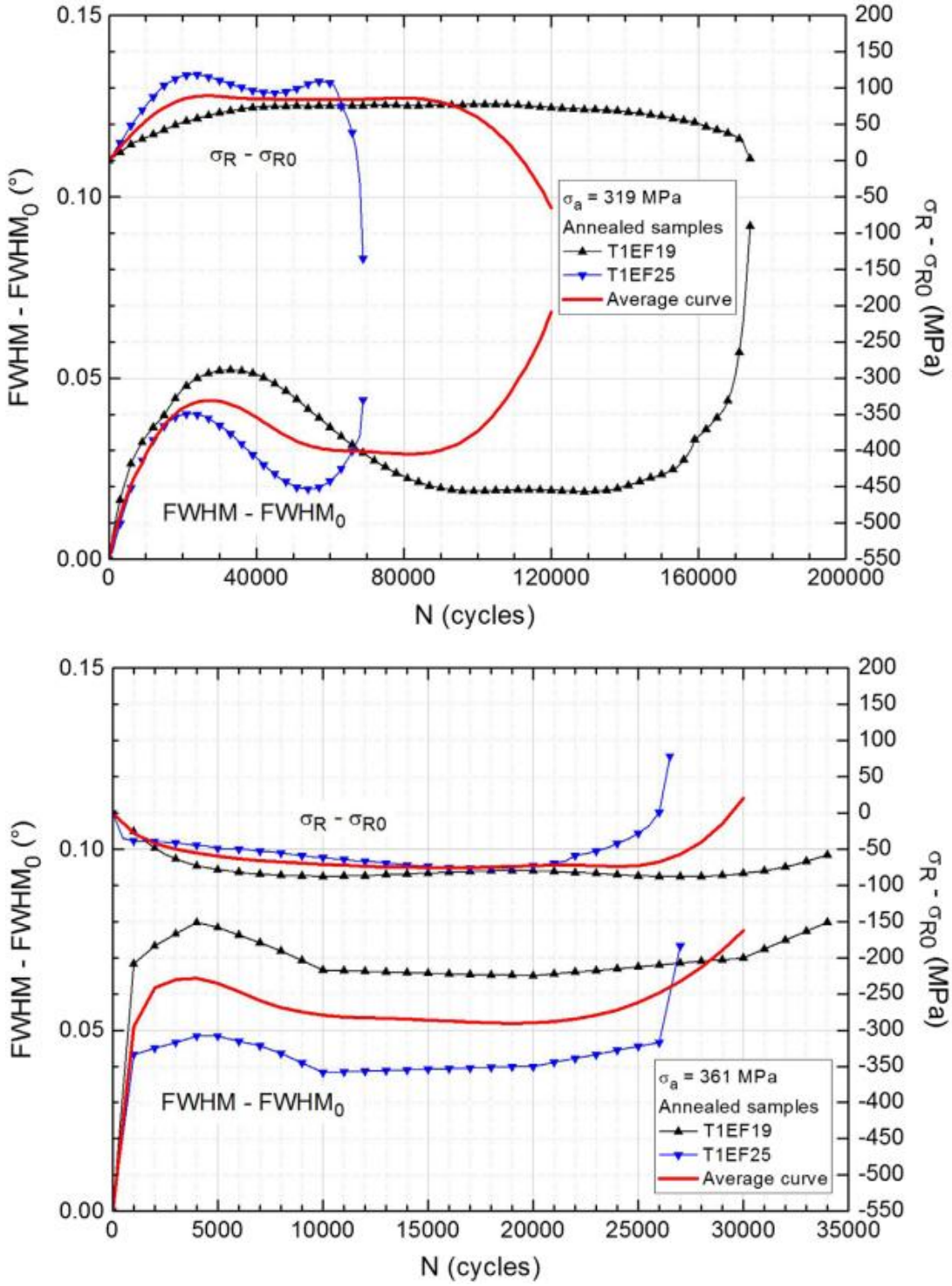

Figure 1.9 - The evolution of FWHM and residual stresses with fatigue cycling on annealed specimens at stress amplitudes of 319 and 361 MPa (R= -1) [7].

Table 1.3 - Fatigue test results of annealed specimens [7].

Specimen	Strain amplitude	Stress amplitude (MPa)		R	N (cycles)
T1EF19	0.17%	319	$0.61\sigma_0$	-1	173,500
T1EF25					68,500

The experimental results found that with the increase of stress amplitude, the variation amplitude of FWHM increased, and the duration of each stage decreased. Unlike the decrease in FWHM observed in the machined specimens, the FWHM of the annealed specimens increased in stages 1 and 3. However, at stage 2, a decrease in FWHM was observed for both machined and annealed specimens.

The rapid increase in the FWHM in stage 1 may be related to the increase of dislocations, the strengthening of interactions, and the hardening of the material. The decrease in FWHM in stage 2 may be related to the rearrangement of the dislocation network and the propagation of microcracks. Finally, the FWHM value of stage 3 is increased until complete rupture.

1.3.2. Electrical resistance testing

The evolution process of fatigue damage is mainly manifested as cyclic microplastic accumulation. The damage manifests as some microcracks on the microscopic scale. From an electronic theory point of view, the resistivity of metals increases with defects such as inclusions, dislocations, vacancies, and micropores. Therefore, according to this theory, we can infer that the resistance of the material should increase with the accumulation of fatigue damage under the continuous action of fatigue. Subsequent research also confirmed this.

Relevant studies have found that under the assumption of conduction load equivalence, damage variables based on resistance changes can effectively characterize the evolution of fatigue damage. This proves that we can predict fatigue damage from the resistance change of the specimen [8].

Experimental procedure: The fatigue test and electrical resistance measurement are performed at the same time. During fatigue testing, DC electrical resistance measurement

was made over the specimen length, using a direct current double bridge for four probes, in which brass screws in conjunction with short and thick copper wires served as electrical contacts [8]. The test machines are shown in the figure 1.10.

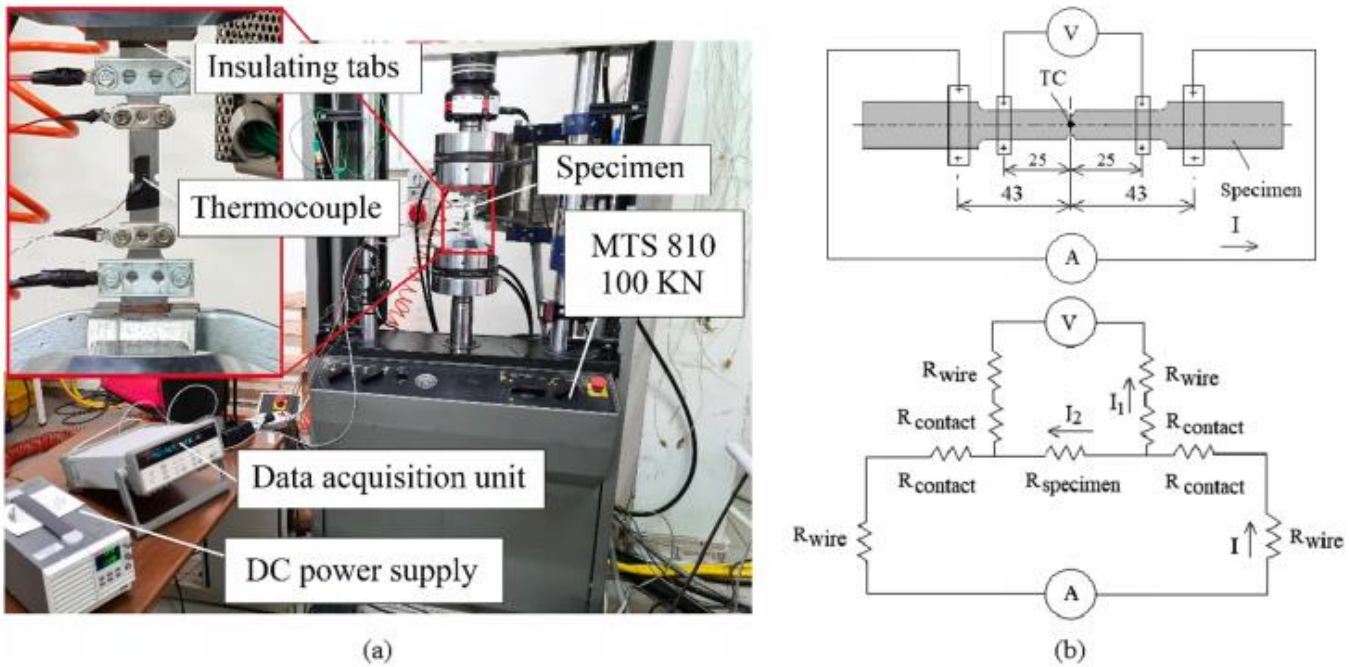

Figure 1.10 - (a) Experimental set-up for electrical resistance measurement and fatigue test; (b) schematic representation of four-wire electrical resistance measurement [9].

Experimental results:

(i) For 45C, 16Mn and 20Mn steel.

The result shows that the predicted values of electrical resistance using equation 2 and the measured values of electrical resistance using equation 3 have the same trend.

$$\frac{R}{R'} = F\left\{1,\frac{4}{3},\frac{7}{3},-2[1-(1-N/N_f)^{\alpha}]^{3/2}\right\} - \frac{2}{3}[1-(1-N/N_f)^{\alpha}]^{3/2} * F\left\{1,2,3,-2[1-(1-N/N_f)^{\alpha}]^{\frac{3}{2}}\right\} \quad (2)$$

$$\frac{R}{R'} = F(1,\frac{4}{3},\frac{7}{3},-2D_M^{3/2}) - \frac{2}{3}D_M * F(1,2,3,-2D_M^{3/2}) \quad (3)$$

Where F is hypergeometric function, N is the number of cycles at a specified stress amplitude and N_f is the number of cycles to fatigue failure at the same amplitude, α is the material parameter, D_M is the maximum damage on the surface of specimen [8].

Figure 1.11 shows the theoretical and test results of resistance change for 45C, 16Mn and 20Mn steels. It can be seen that in the initial stage of fatigue, the resistivity of the material increases slowly with the number of cycles, and when it reaches a critical value, the resistivity increases suddenly, corresponding to the fracture failure of the specimen. It is also observed that the larger the fatigue load amplitude , the faster the resistivity changes.

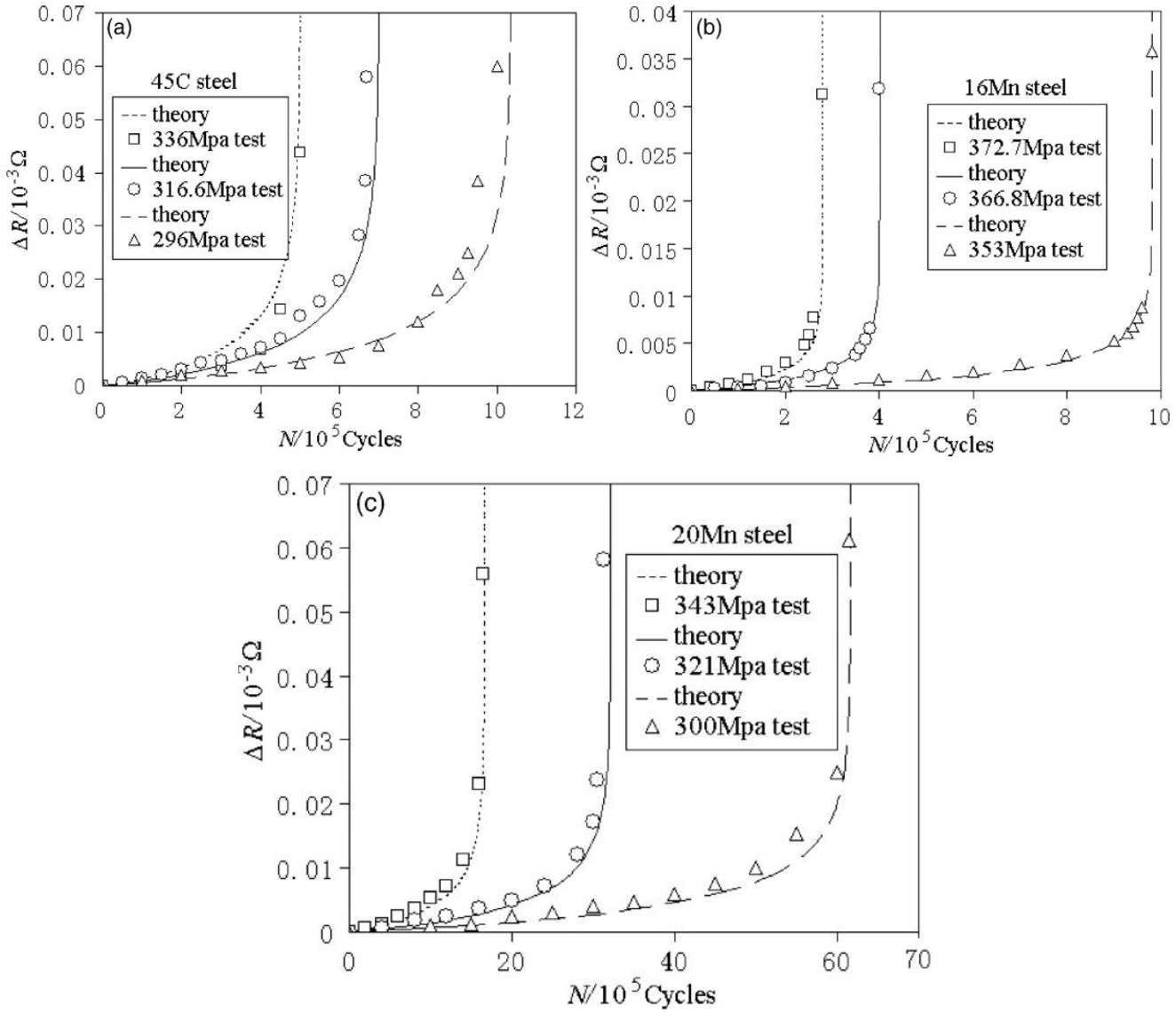

Figure 1.11 - Experimental results of electrical resistance change of 45C, 16Mn and 20Mn steel:
(a) - 45C steel, (b) - 16Mn steel, (c) -20Mn steel [8].

(ii) AISI 316L stainless steel

From the experimental results in Figure 1.12, it can be seen that there is an overall trend of rapid increase in resistance for all specimens when reaching about 20-40% of the fatigue life time. The increase in electrical resistance is associated with fatigue damage, which results in an increase in the resistivity of the material located in the region where the notch is located. Subsequently, a general trend of rapid increase in resistance was observed at approximately 65-75% fatigue life, and the increase in resistance became more pronounced at approximately 80% fatigue life [10].

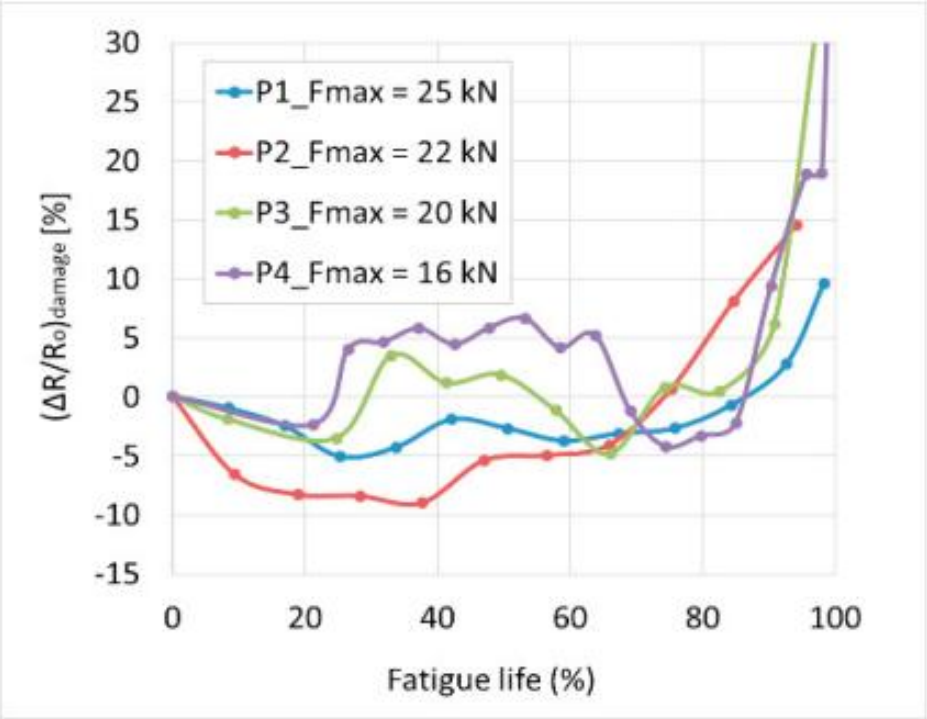

Figure 1.12 - Experimental results of electrical resistance change of AISI 316L stainless steel [10].

1.3.3. Acoustic emission technique

Acoustic emission (AE) is a passive nondestructive testing technique. It is a detection method by detecting elastic waves generated by irreversible changes in the internal structure of materials. For example, a sudden redistribution of stress within a material due to aging, temperature changes, or external mechanical forces, etc., converts mechanical energy into acoustic energy. Some examples of elastic stress waves that can be emitted are

plastic deformation, creep, nucleation and propagation of fatigue cracks, and fracture of inclusions [11].

It should be noted that there are many factors that affect the sound source, such as gratings between crack surfaces, friction of moving parts, hammering, vibration, temperature, etc. Therefore, when collecting acoustic emission signals, it is easy to collect interference signals, and some thresholds are usually set to eliminate noise.

The advantage of the acoustic emission method is that it is a passive method that uses sensors to detect elastic stress waves. It does not require a full scan of the structure, only the correct number of sensors to detect the resulting signal, so it is suitable for continuous structural health monitoring (SHM) [12].

Research work by Roberts and Talebzadeh used AE signals to estimate crack growth based on the empirical relationship between acoustic emission count rate and crack growth [13,14]. In the research work of Yu J, Keshtgar, and Modarres [15,16], crack growth and fatigue life prediction were performed based on count rate and absolute energy rate.

The test machines are shown in the figure 1.13.

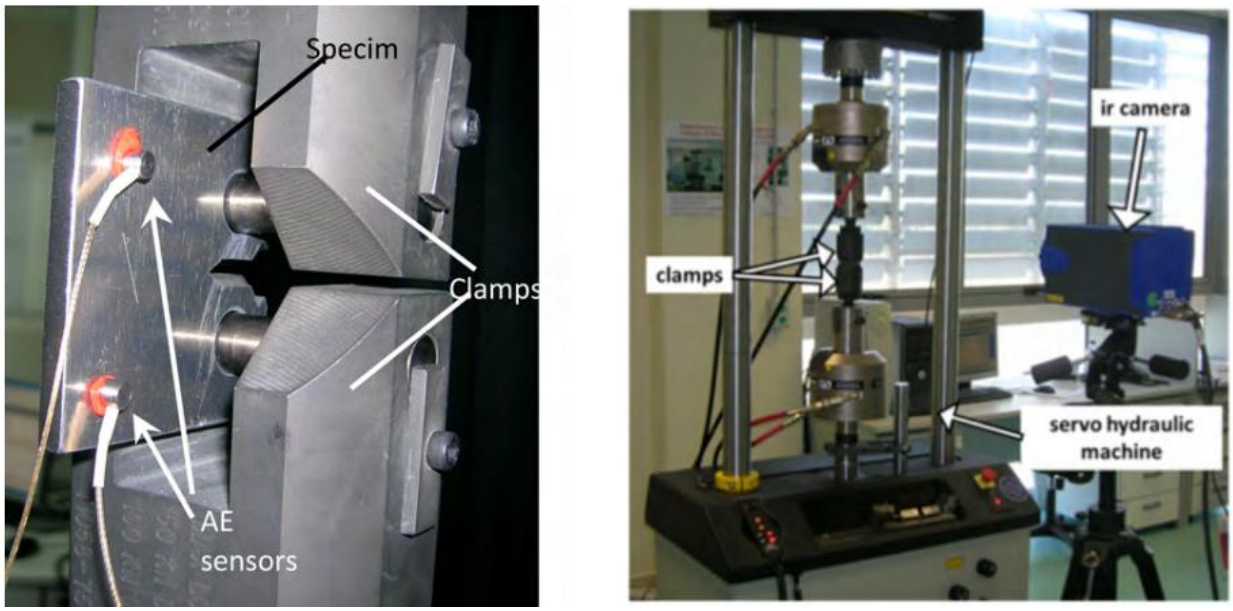

Figure 1.13 - Fatigue test machine and the acoustic emission sensors on the specimen[15].

Experimental procedure:

Fatigue test and acoustic emission were carried out simultaneously. To collect data, two sensors are mounted on one side of the sample. At the same time the sensors are

connected using wax, which enhances the acoustic coupling. Record the entire waveform data for post data processing.

Experimental results for structural steel:

In order to predict crack length and residual fatigue life, the values of C, Be and p need to be obtained, which need to be combined with AE monitoring using standard samples for fatigue testing. After obtaining these constant values under specific loading conditions for a representative material used in an actual structure (Table 1.4), equation (4) can be used to predict crack length and residual fatigue life.

$$\frac{da}{dN} = D\left(\frac{dU}{dN}\right)^{q} \qquad (4)$$

where $D = C/(B_e^q)$, $q = m/p$. dU/dN is AE absolute energy rate, da/dN is crack growth rate [15].

From Figure 1.14, it can be seen that there is a certain deviation in the experimental data at the beginning due to the residual stress of the pre-crack. Experimental data from the CT2 test showed a distinct jump in the middle, which was caused by increased cyclic loading.

As shown in Figure 1.14 and Table 1.4, the cumulative absolute energy rate varies in three stages. During the first phase, when fatigue begins, the cumulative absolute energy rate increases by a small amount. Subsequently, the cumulative absolute energy rate of the second stage is basically unchanged. In the final third stage, when the fatigue cycle reaches a certain value, the cumulative absolute energy rate increases rapidly. After the crack length exceeds the critical level, the increments of the cumulative absolute energy and cumulative count become significantly larger [15].

Table 1.4 - Crack growth and AE constants for specimens CT1, CT2 and CT3 [15].

Specimen	Thickness	Load ratio	AE absolute energy rate			AE count rate		
			p	log(B_e)	B_e	p_n	log(p_n)	B_n
CT1	12.7	0.02	5.7489	-10.865	1.36E-11	4.9062	-10.91	1.23E-11
CT2	19.05	0.1	5.7867	-9.9986	1.00E-10	5.1263	10.755	1.76E-11
CT2	12.7	0.1	5.9154	-11.173	6.71E-12	4.6235	-9.9154	1.22E-10

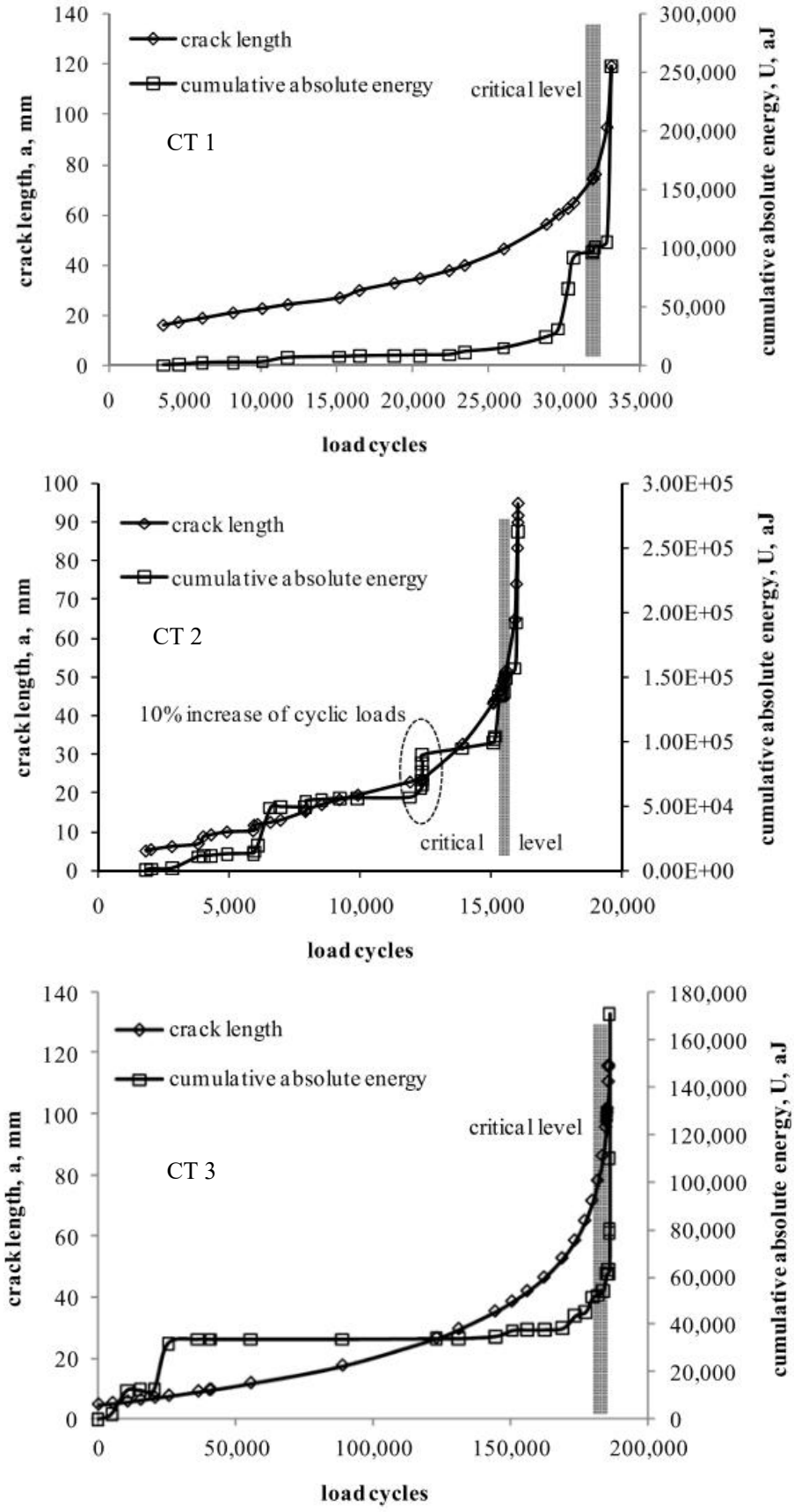

Figure 1.14 - The result of crack length and AE cumulative absolute energy versus load cycles of different specimens [15].

1.3.4. Micro-hardness testing

According to Ye and Wang [17], fatigue damage in the early stage of material fatigue crack propagation is mainly related to the plastic strain concentration that occurs and develops at or near the material surface during cycling. Therefore, it is of great significance to study the fatigue damage accumulation of materials by studying the changes of material surface microhardness. This method of studying fatigue damage provides a new method for the prediction of fatigue life before macroscopic cracking of materials. The test machine is shown in Figure 1.15.

Figure 1.15 - Fatigue test machine and HXD-1000 micro hardness tester.

Experimental procedure: Fatigue tests and microhardness measurements were performed simultaneously. First, the fatigue test is carried out with a fatigue testing machine under the set load amplitude and number of cycles until the specimen fails. To measure the microhardness of the specimens during the fatigue process, the fatigue test was interrupted after different selected number of cycles, 10 interruptions for each specimen before failure, and a HXD-1000 microhardness tester and a diamond conical indenter were used to measure Vickers microhardness on the sample surface.

And considering the chemical and structural inhomogeneity of the material, 25 microhardness measurements were randomly done on the surface of the smallest cross-section of the sample, and then the measurement results were statistically processed [18].

Experimental results:

(i) Annealed 16Mn steel

As shown in Fig. 1.16, in the high cycle fatigue process, the average value of the Vickers microhardness of annealed 16Mn steel first increases at the initial stage of fatigue loading, and the microhardness reaches the maximum value after a certain number of cycles, and then the microhardness increases. The gradual decrease corresponds to the first hardening and then softening of the sample surface.

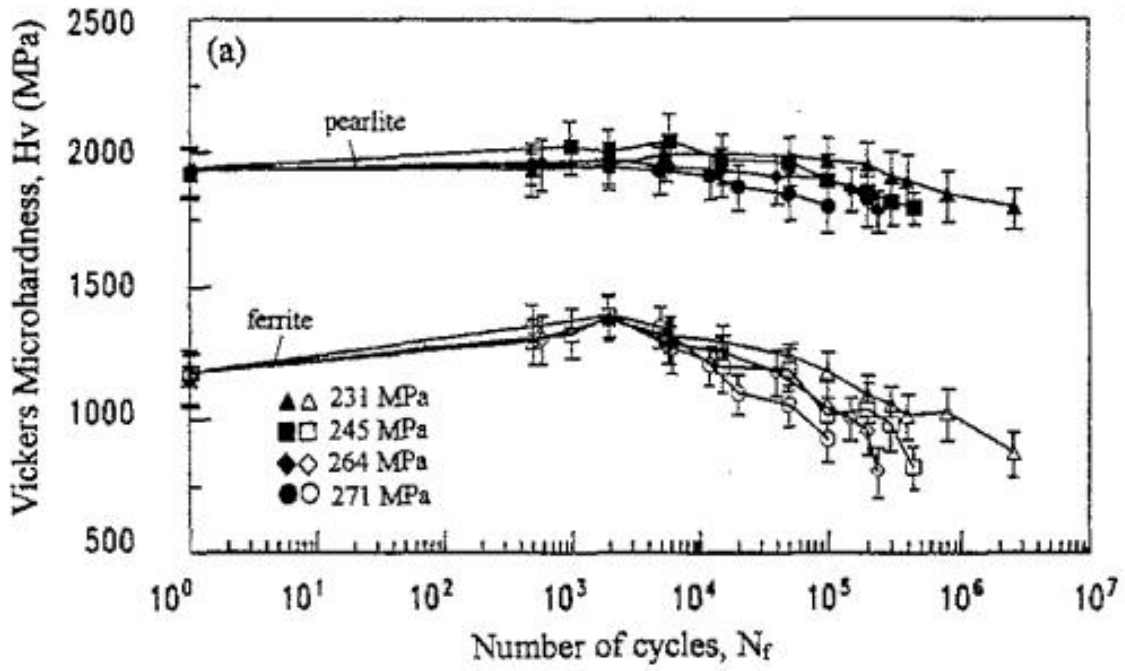

Figure 1.16 - Micro hardness change of annealed 16Mn steel [18].

(ii) Normalized 45 steel

The average value of the normalized 45 steel microhardness for ferrite-pearlite composites decreases slightly in the initial stage, followed by an increasing process. After reaching a maximum value, it decreases asymptotically with increasing number of cycles. The change in microhardness mainly corresponds to the initial softening of the surface

material, after a certain number of cycles, hardening begins, and then softens again later in the cycle.

As shown in the figure 1.17. The normalized 45C steel, the mean value of microhardness is characterized by a slight decrease in the initial stage of fatigue action, then a gradual increase, and after reaching a maximum value, it decreases with increasing number of cycles. The change in microhardness mainly corresponds to the initial softening of the surface material, after a certain number of cycles, hardening begins, and then softens again later in the cycle[18].

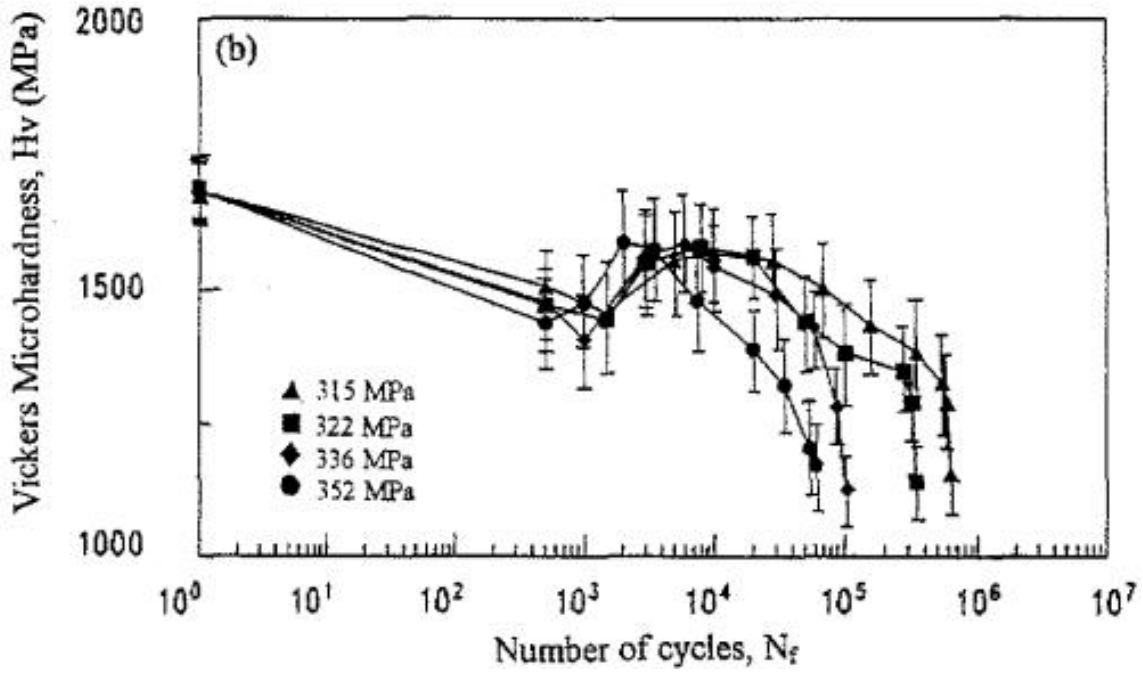

Figure 1.17 - Micro hardness change of normalized 45C steels [18].

(iii) annealed 0.46% carbon steel (45C steel)

For annealed 45 steel (Fig. 1.18), the average microhardness values of ferrite and pearlite show three stages of increase, stabilization and decrease during high cycle fatigue. Pearlitic microhardness has a shorter duration of stabilization, about 1% of the overall fatigue life, which is related to controlled stress levels. Most of the fatigue life is spent in the microhardness reduction stage. It is observed that the mean square deviation of

microhardness exhibits a rising and falling characteristic during fatigue life, and the deviation of pearlite is larger than that of ferrite [19].

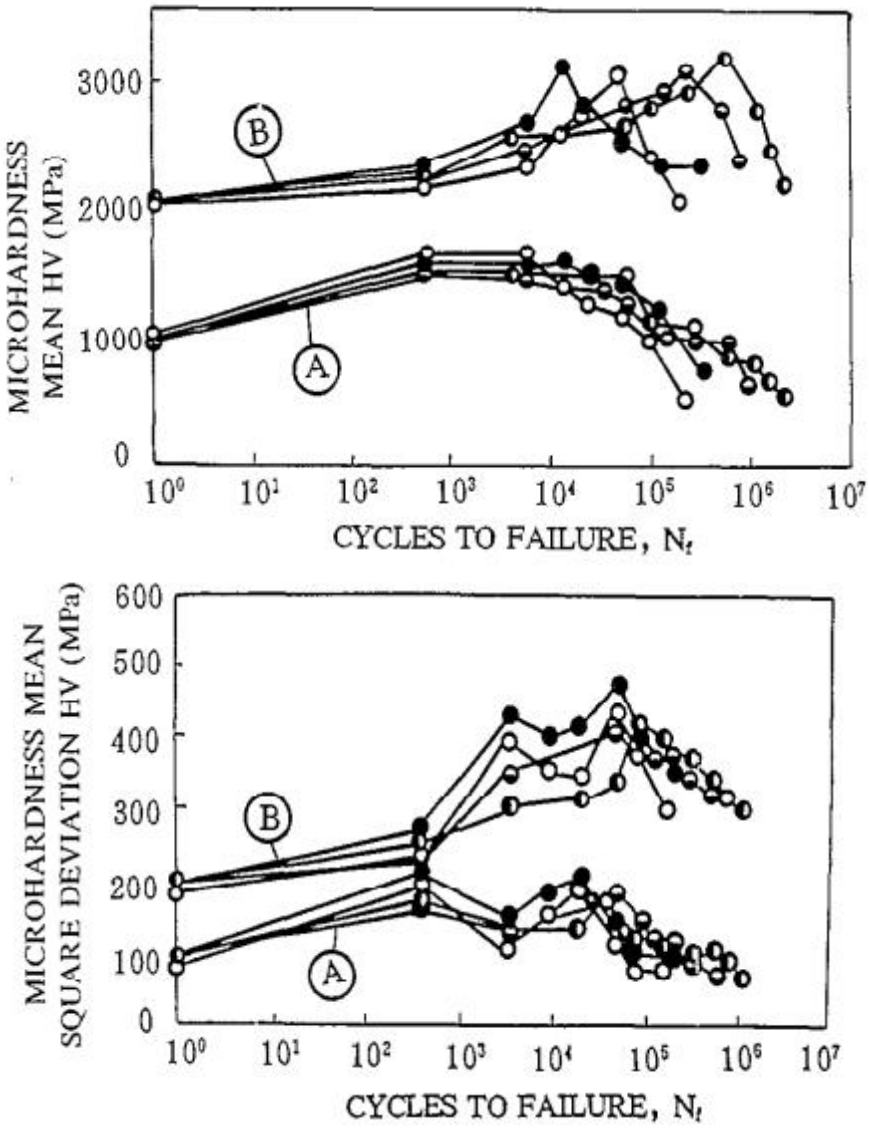

Figure 1.18 - The change of micro-hardness mean and mean square deviation of annealed 45C carbon steel ferrite and pearlite during fatigue: (A) ferrite; (B) pearlite. ◐ 200 MPa; ◒ 220 Mpa; ● 240 Mpa; ○ 260 Mpa [19].

Conclusion to part 1

In this part, the linear methods of fatigue life determination were studied first, and found that it has many shortcomings to predict the residual fatigue life of material. Then the nonlinear methods were introduced.

And the existing research works shows that it is possible to apply nondestructive testing to study the change of mechanical properties of materials, such as X-ray diffraction, electrical resistance testing, acoustic emission and microharness testing. By studying the nonlinear behaviour of mechanical properties of materials, it is possible to predict the residual fatigue life of materials.

And it is found that when the nonlinear behavior of the material is relatively simple, using a non-destructive testing technique to obtain the change of material properties is sufficient to predict the residual fatigue life. But it should be known that when the nonlinear behavior of the material is relatively complex, only analysis one property change to predict residual fatigue life is complex. Therefore, it is proposed that the prediction of fatigue life can be made more accurate through different non-destructive testing methods combined with the changes of various properties of the material, which will be studied later in this work.

2. EXPERIMENTAL PROCEDURE AND TEST MACHINES

2.1. Materials and test specimen

The specimens are aluminum alloy Д16Т plates with a thickness of 1.24 mm. Sheets are delivered with normal manufacturing precision and heat treatment. The material is artificially aged to mimic aircraft materials in use. Obtain the desired geometry, including fillets, by milling. After the flight simulation is loaded, cut smaller samples with a hacksaw to a width of 0.4 mm.

The mechanical properties of the materials are shown in Table 2.1. The chemical composition is shown in Table 2.2.

Table 2.1 - Mechanical characteristics of D16T material.

Material	Tension strength limit,MPa	Yield limit, MPa	Poisons ratio,%	Modulus of elasticity, MPa
D16T	430	300	10	0,71

Table 2.2 - Chemical composition in % of D16T aluminum alloy.

Chemical compound of aluminium alloy, %										
Si	Fe	Cu	Mn	Mg	Cr	Zn	Ti	Other		Aluminium
								Separately	Summary	
0,50	0,50	3,8	0,30	1,2	0,1	0,25	0,15	0,05	0,15	Residual

The geometry of the specimen is shown in Figure 2.1. This shape makes the stress distribution of the critical section uniform. The specimen has three holes as stress concentrators to simulate rivet holes in the skin of an aircraft, with a diameter of 3 mm.

Fatigue cracks usually occur at the location of the greatest stress concentration, and three holes in the specimen replace this stress concentration. And the maximum stress concentration factor is equal to 2.57.

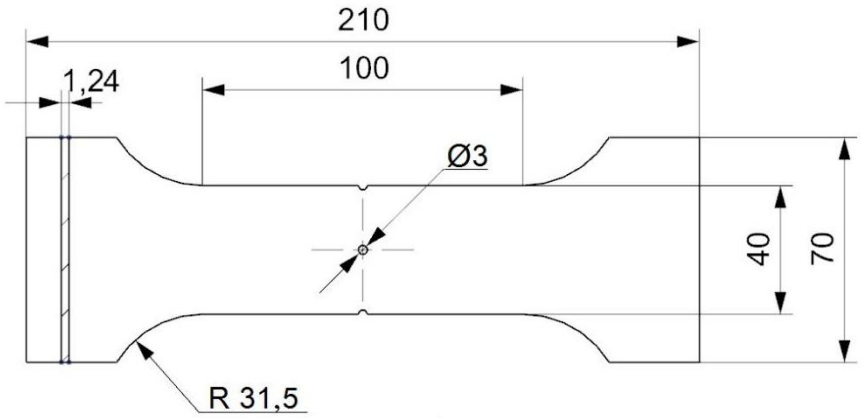

Figure 2.1 - Geometrical shape of specimen.

2.2. Servo Hydraulic BiSS fatigue test machine

Fatigue tests were conducted on the test machine Bi-00-202V. The design and functional architecture of the test machine with digital control Bi-00-202V consists of four parts (Figure 2.2):

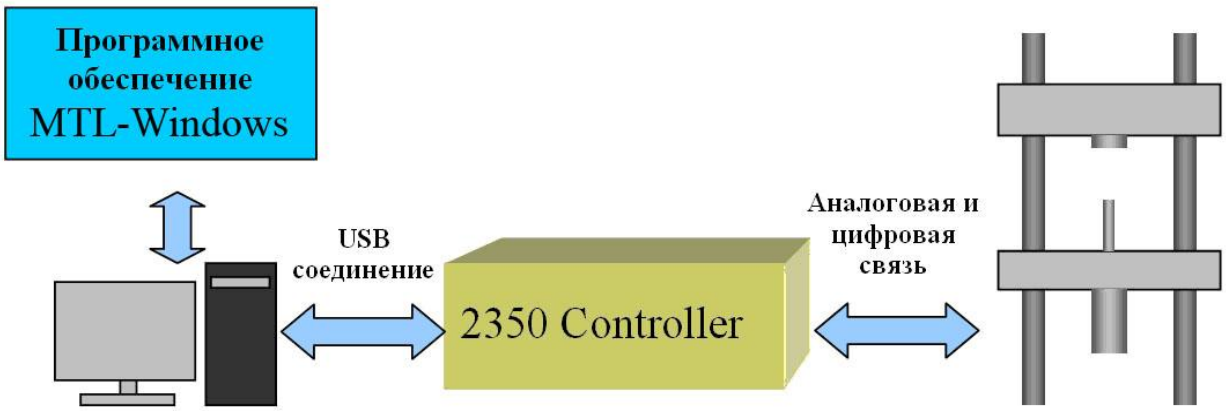

Figure 2.2 - Architecture of test machine Bi-00-202V.

(1) MTL-Windows software;

(2) Personal computer (PC);

(3) Digital-to-analog converter 2350-Controller;

(4) Testing machine.

The system characteristics of the personal computer meet the requirements (not lower): Intel PIII @ 800 MHz or its equivalent; 128 MB of RAM; 20 GB of hard disk

space; USB interface support. The operating system on the PC must be at least Windows-98.

The design of the testing machine (Figure 2.3) has a rigid scheme formed by the base, columns and the upper traverse.

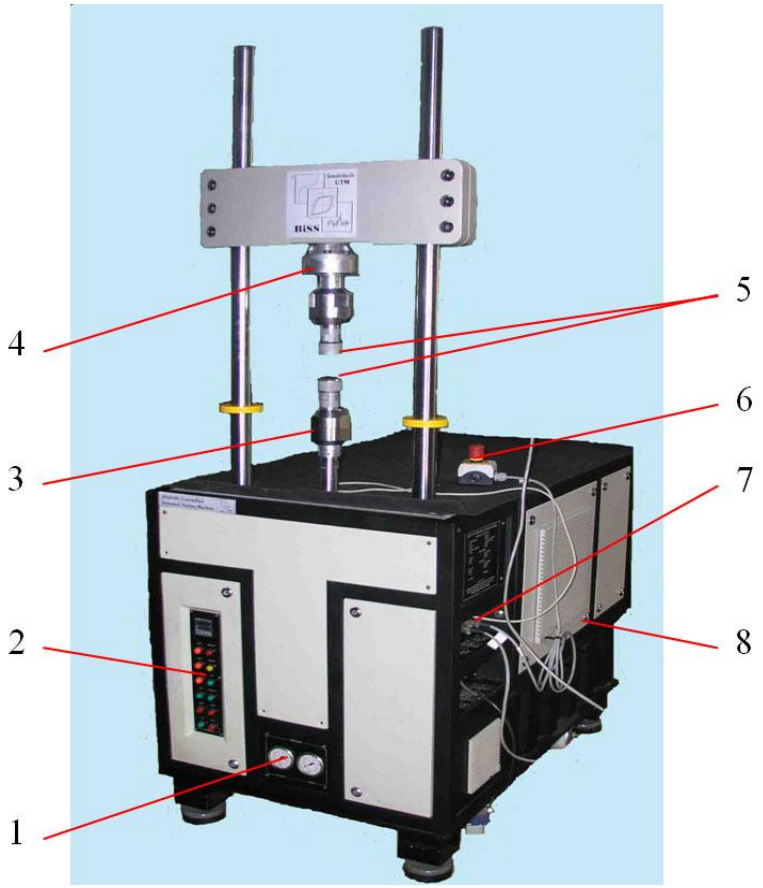

Figure 2.3 - Main structures of the test machine:

1 - Pressure gauges of the hydraulic system; 2 - Electricity supply network; 3 - Executive mechanism; 4 – Load cell; 5 – Grips; 6 - Emergency stop button; 7 - Connectors for sensors and USB ports; 8 - 2350 Controller.

The strain gauges are attached to the upper fixed beam (4). The load of the specimen due to the movement of the rod of the actuator (3). The test program code specified in MTL-Windows is transferred as a digital signal from the PC to the DAC 2350-controller via the USB port. The device receives input digital signals and converts them into analog and digital signals for commands to control the hydraulic system. In turn, the hydraulic system controls the movement of the actuator's rod (3).

Three information exchange channels are used to control the testing machine:

(1) The movement channel of the actuator rod. The working range is ±50 mm and the accuracy is 0.001 mm;

(2) Loading channel. The operating range is ±25 kN and the accuracy is 0.001 kN;

(3) Extensometer channel. The working range is ±0.5 mm and the accuracy is 0.0001 mm.

Sample loading can be done using one of the three channels, which in this case will be the active control channel. The other two monitoring channels work in message transfer mode.

Data on the load of the specimen is displayed in the interface of the MTL-Windows software (Figure 2.4).

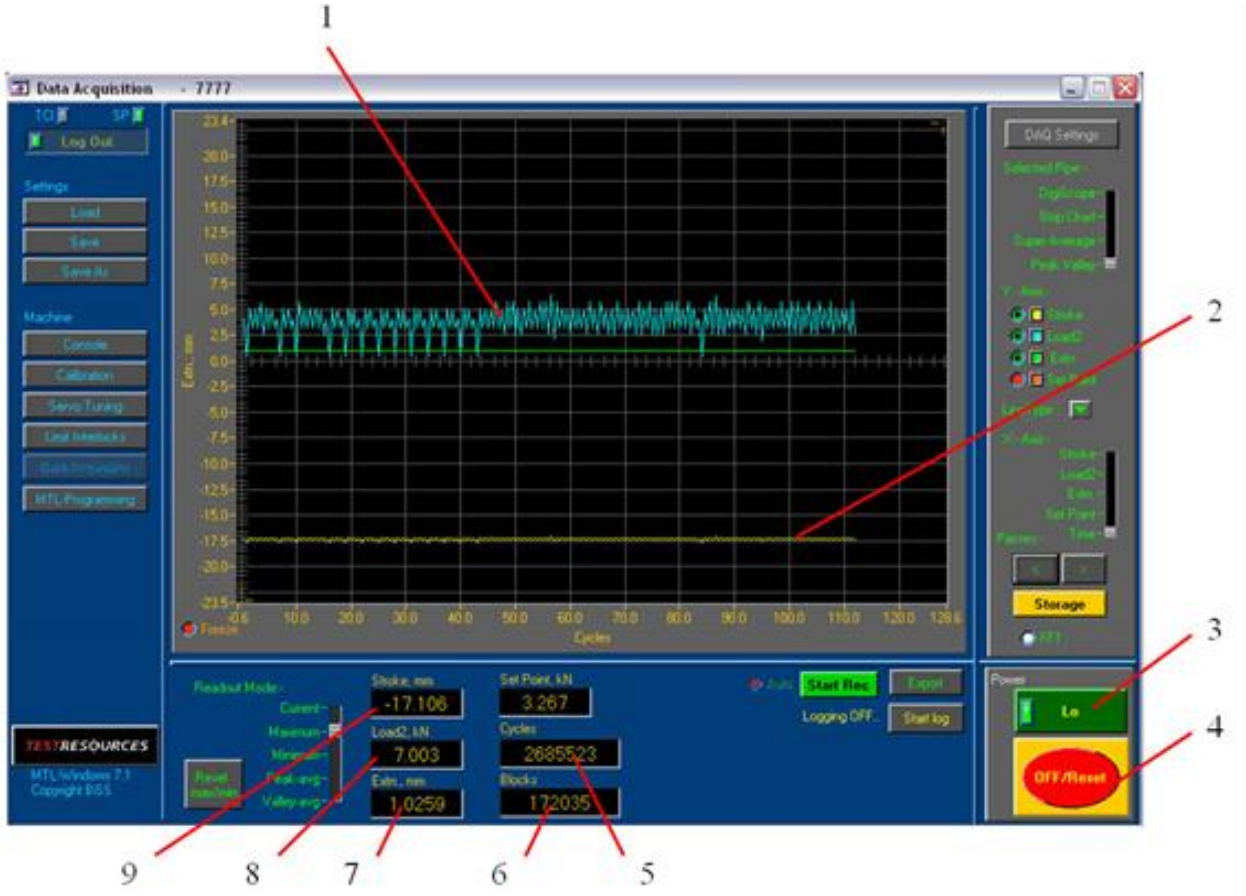

Figure 2.4 - The MTL-Windows software application:

1 - load spectrum displayed in real time; 2 - movement of the rod; 3 - power button; 4 - shutdown button; 5 - load cycle counter; 6 - counter of blocks / flights; 7 - extensometer indicator; 8 - load indicator; 9 - indicator of the position of the rod of the executive mechanism

The signals in the control channel are formed as follows: The analog signals from the rod position sensor, dynamometer and extensometer are transmitted to the DAC 2350 controller, where they are converted into digital signals and sent to the PC, and then displayed in the MTL-Windows software interface.

The information received from the three control channels can be used to form or change the control signal of the active control channel, which is a necessary condition to achieve a random load spectrum.

2.3. Microhardness tester PMT-3M

For the microhardness testing the PMT-3M was used. The main components of the microhardness tester PMT-3M are show in the figure 2.5.

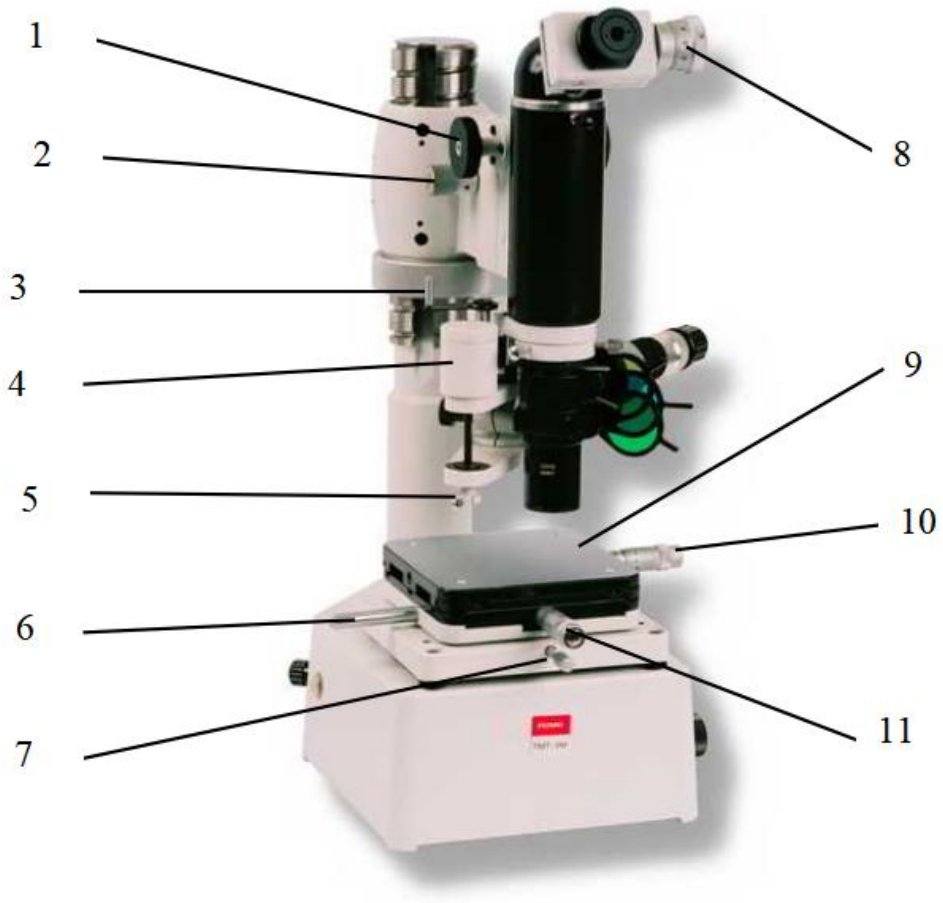

Figure 2.5 - General view and main components of microhardness tester PMT-3M.

(1) Coarse adjusting nut: it can moved up and down the tube coarse;

(2) Micrometric adjusting nut: it can moved up and down the tube micrometric;

(3) Indenter handle: Slowly turn the handle clockwise to lower the rod so that the diamond contacts the surface of the specimen;

(4) Loading: it has a weight of 100 gram;

(5) Diamond: it will come into contact with the surface of the specimen and leave an indentation;

(6) Base handle: it can rotate the base;

(7) Base fix screw: it secures the base and prevents it from turning when pressure is applied;

(8) Eyepiece micrometer: It can measure the size of the indentation on the surface of the specimen;

(9) Plate: Specimen will be placed on it and be tested;

(10) Left and right adjustment screw: It can fine-tune the base plate left and right;

(11) Front and rear adjustment screw: It can fine-tune the base plate front and rear.

The experimental procedure to use microhardness tester PMT-3M are:

(1) Put the specimen on plate 9 so that it the investigated surface is located parallel to the working the plane of the table on which the plate with the specimen being tested. The surface of the item to be tested should be flat, clean, with a roughness not coarser than grade 9 category "a", i.e. the arithmetic mean profile deviation - (Ra) – should not be more than 0.32 microns;

(2) Place a load on the thickened part of the rod;

(3) Choose a place on the specimen to be imprinted. Distance from the center of the print to the edge of the specimen or between the centers of adjacent prints should be at least three lengths of the print diagonals, the minimum the thickness of the specimen or layer must exceed the depth of the imprint not less than 10 times. In the study of individual structural constituent metal alloys, the same rules apply;

(4) Using the handle 6, smoothly turn the object stage against clockwise until it stops, avoiding jerks when leading to emphasis. Fix the table in this position with screw 7;

(5) Slowly turn the indenter handle 3 counterclockwise lower the rod so that the diamond touches the surface of the test subject. Rotate the handle approx. 180° within 10-15 sec. After holding for 5 sec. turn under load handle to its original position;

(6) Release screw 7, turn the stage back position to the stop. To avoid hitting the stop and shifting object relative to the set position, the table must be turn very carefully;

(7) Measure the diagonal of the print using the eyepiece micrometer. By screws 10 and 11 of the table and by rotating the drum eyepiece micrometer 8 bring the center of the crosshairs to one edge of the imprint diagonal (Figure 2.6a) and read the scales eyepiece micrometer.

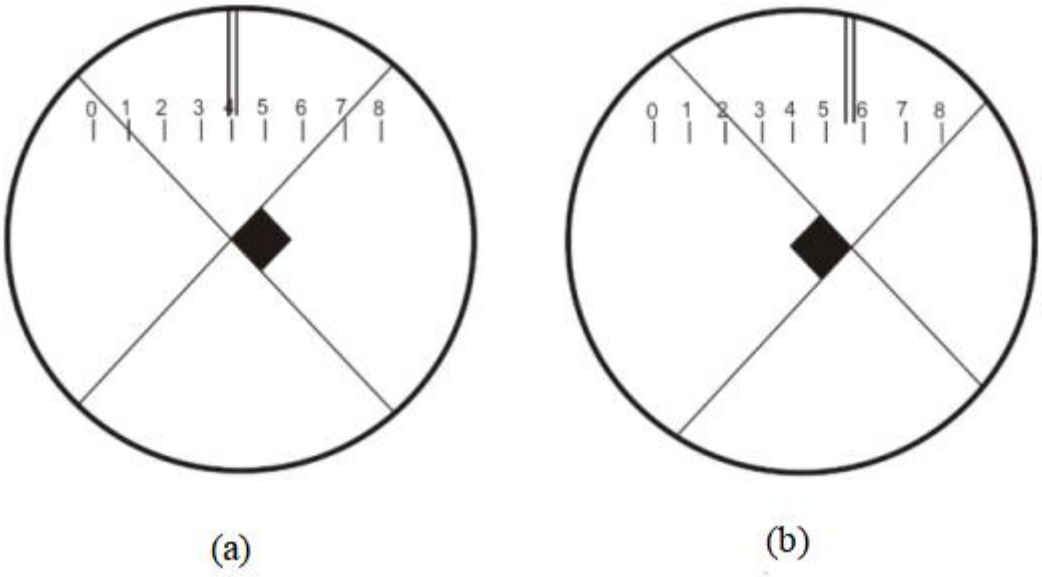

Figure 2.6 - Scheme for measuring the imprint.

Then, by rotating the drum of the ocular micrometer in the same side (by moving the center of the crosshair along the diagonal of the print) align the center of the cross with the second edge of the diagonal (Figure 2.6b) and read again on the scales of the ocular micrometer.

Difference of readings, multiplied by the actual value of the price division of the drum, will give the true value of the diagonal of the print.

The microhardness number can be calculated by the formula 5:

$$HV = \frac{1854P}{d^2} \qquad (5)$$

Where P (100 g) is the normal load applied to the diamond tip, N (kgf); d is the arithmetic mean of the lengths of both diagonals of a square imprint, mm.

Conclusion to part 2

The aluminum alloy Д16Т is chosen to do the fatigue tests and microhardness tests. And the geometry of the specimens are defined. Fatigue tests were conducted on the test machine Bi-00-202V, and for the microhardness testing the PMT-3M was used. The experimental procedure to use PMT-3M microhardness tester was also introduced.

3. EXPERIMENTAL RESULTS AND DISCUSSION

3.1. Standardized load spectra and load-time histories

For fatigue test in this work, the TWIST loading spectrum[21] was used. And the details of standardized load sequence - TWIST is shown in the table 3.1.

It is well known that fatigue behavior data and models of materials and structures under constant amplitude loads may not be suitable or sufficient to adequately evaluate their fatigue performance under irregular variable amplitude loads. Therefore, it is generally accepted that realistic load spectra need to be applied in order to gain a realistic understanding of the fatigue behavior of materials and structures under irregular variable amplitude loads. The currently available Standardized Load Order or Load Time History (SLH) provides an appropriate load order selection for this purpose [20].

Table 3.1 - The details of standardized load sequence - TWIST [20].

standardized load sequence - TWIST	
Purpose	Transport aircraft wing root
Description of load history	Constant. positive mean stress for gust loads, ground-air-ground cycles (GAG)=under-loads
No. of load components or additional variables (time, temperature, etc.)	1
Block size (cycles)	402000
Equiv. usage	4000 flights
Spectrum shape factor	3.09
No. of load level	20

Standardized load sequences or load-time histories (SLH) are often used to validate numerical fatigue life predictions and provide input for those interested in studying cumulative damage effects, as they may need to apply multiple load series with different characteristics in order to clarify Validity of models and assumptions. Typically, SLH is only defined as a representative portion of the spectrum, i.e. does not cover the entire

serving spectrum. Therefore, the spectrum is considered to be repeated in tests or numerical simulations until eventual failure.

The TWIST load spectrum is by far the most widely used load spectrum in fatigue studies of transport aircraft wings, not because it represents the loads on the lower wing root of a transport aircraft, but because it contains frequent loads [20]. A unique feature of the TWIST load spectrum is the presence of a uniformly distributed load level spectrum [22]. Unlike most other load spectra, even the smallest magnitude load cycles in TWIST can cause up to 20% fatigue damage, even though they may be below the fatigue threshold. This capability makes TWIST an excellent choice for variable amplitude fatigue studies, as it allows the evaluation of the sensitivity of individual load levels to load interactions under biaxial loading [23].

The aerodynamic lift on the wings of an aircraft carries the weight of the entire aircraft. This distributed load imposes a bending moment on the wing and is greatest at the root of the wing. On the ground, the lift is zero and the aircraft is supported by the landing gear. Therefore, each flight means a cycle of bending moments on the wing, as shown in Figure 3.1.

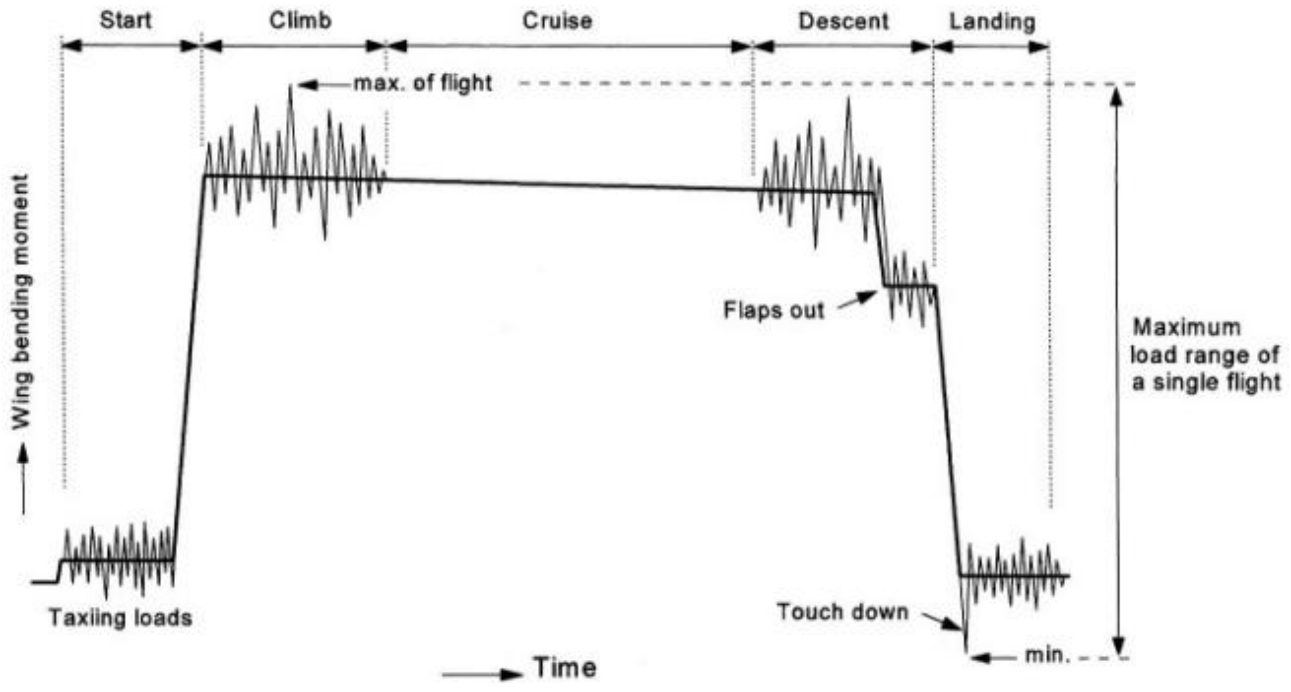

Figure 3.1 - Wing bending moment during a single flight [3].

The bending of the wing introduces tensile stress in the skin structure on the lower surface of the wing and compressive stress in the skin structure on the upper surface of the wing. Tension skin is considered a critical part of wing fatigue. Each flight cycle on the tension skin is a very slow cycle with almost quasi-static changes in load. However, the wings also experience faster load cycling in turbulent air (gust weather), mainly during low altitude climbs and descents [3].

The TWIST spectrum consists of 4,000 different flights (about 3.94 ×105 cycles) and 4,000 landings to simulate the load spectrum of a transport aircraft wing [24]. The loads in the spectrum are characterized by the mean flight stress S_{mf}. The TWIST spectrum is defined by mission type and flight load level. That is, according to the task segment during the flight, it is divided into 10 categories. And divide the load of each task segment into 10 levels [25], as shown in Table 3.3. The loading order of each level is randomly generated, and the following statistical results can be obtained: as shown in Table 3.2.

Table 3.2 - Occurrence number at different load levels and different flight types in TWIST [25].

Flight type	Load level									
	I	II	III	IV	V	VI	VII	VIII	IX	X
	1.6	1.5	1.3	1.15	0.095	0.84	0.685	0.53	0.375	0.222
FT_A	1	1	1	4	8	18	64	112	391	900
FT_B		1	1	2	5	1	39	76	366	899
FT_C			1	1	2	7	22	61	277	879
FT_D				1	1	2	14	44	208	680
FT_E					1	1	6	24	165	603
FT_F						1	3	19	115	512
FT_G							1	7	70	412
FT_H								1	16	233
FT_I									1	69
FT_J										25
F_i	1	2	5	18	52	125	800	4170	34800	358665

Note: F_i means total cycle number during 4000 flights.

The Figure 3.2 shows the samples of the TWIST load sequence, the TWIST spectrum (40,000 flights) consisting of gust, ground-air-ground and taxiing load elements.

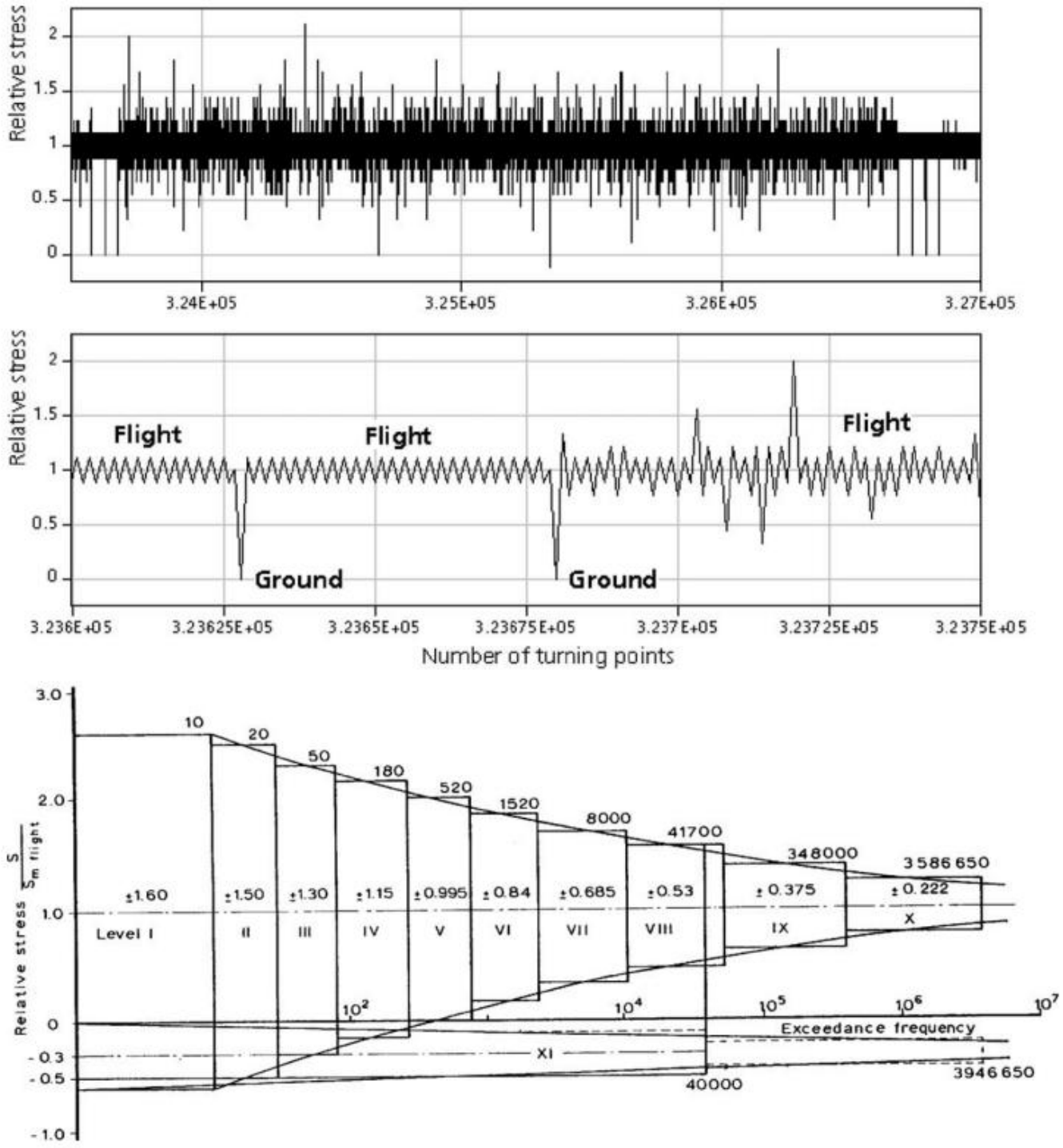

Figure 3.2 - Samples of the TWIST load sequence (top) and the TWIST spectrum (40,000 flights) consisting of gust, ground-air-ground and taxiing load elements(bottom) [20].

Table 3.3 - Overview of the 10 load levels of the TWIST load spectrum [26].

Load level	Load factor LF	Stress ratio R	Load cycles n
I	±1.6	-0.23	1
II	±1.5	-0.20	2
III	±1.3	-0.13	5
IV	±1.15	-0.07	18
V	±0.995	0.00	52
VI	±0.84	0.09	125
VII	±0.685	0.19	800
VIII	±0.53	0.31	4170
IX	±0.375	0.45	34800
X	±0.222	0.64	358665

3.2. The result of microhardness testing

For the microhardness testing the PMT-3M was used. In this work, two specimens were used for a total of 52,002 cycles. The microhardness measurement interval is approximately 4000 cycles. In order to eliminate errors, a total of 10 microhardness measurements were carried out in each interval, and the average value of the 10 measurement results was taken as the microhardness of this cycle. The experimental results are shown in Table 3.4. and the experimental results of deviation of microhardness is shown in the Figure 3.4.

Table 3.4 - The experimental results of average value of microhardness.

Number of cycles	Specimen 1		Specimen 2	
	Average	deviation	Average	deviation
0	122.9	3.3	127.5	3.1
4004	125.2	1.9	120.5	2.8
8001	114.2	2.7	105.6	3.1
12006	100.1	6.1	103.7	9.3
15999	103.4	3.0	113.5	2.7
20006	116.8	2.9	98.2	4.1
24005	121.4	3.4	109.5	8.9
27999	119.6	3.4	117.5	2.7
32005	115.4	1.8	117.3	1.3

Continue to Table 3.4

36004	121.4	3.0	112.9	4.3
40002	122.9	1.9	125.9	3.1
44004	117.5	2.3	112.8	2.5
48002	122.3	2.5	120.1	2.8
52002	114.3	3.3	122.4	4.2

Figure 3.3 - The experimental results of average value of microhardness.

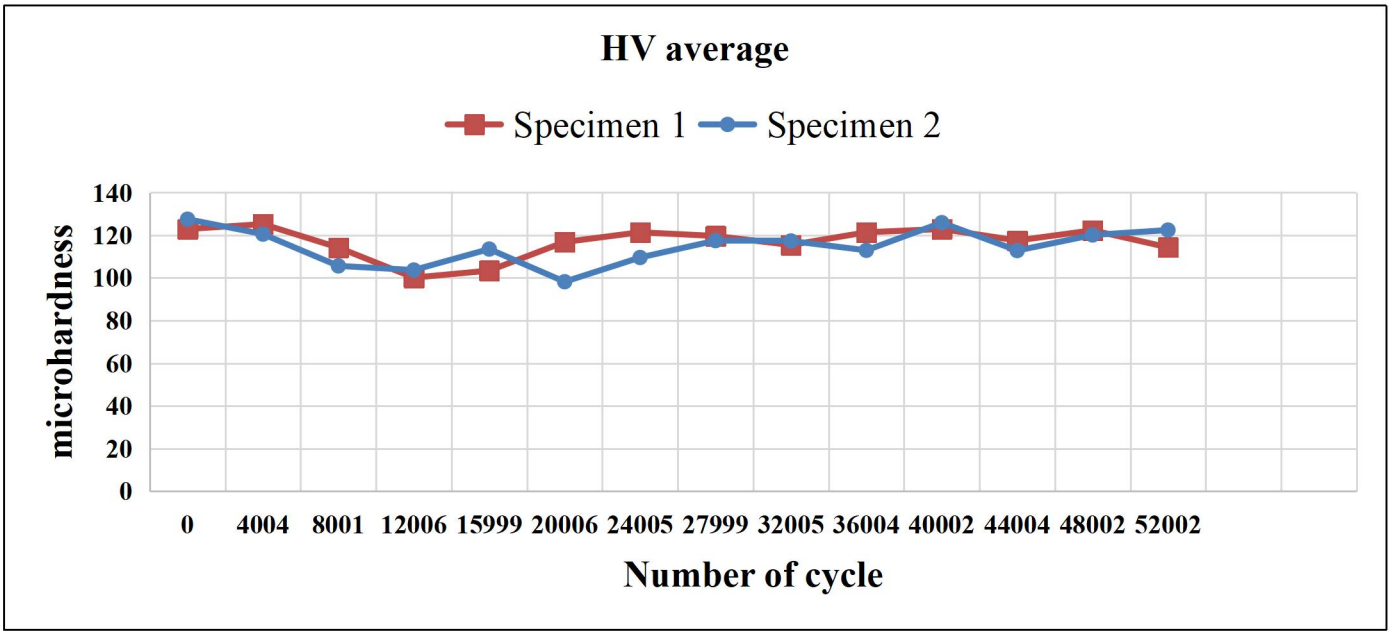

Figure 3.4 - The experimental results of deviation of microhardness.

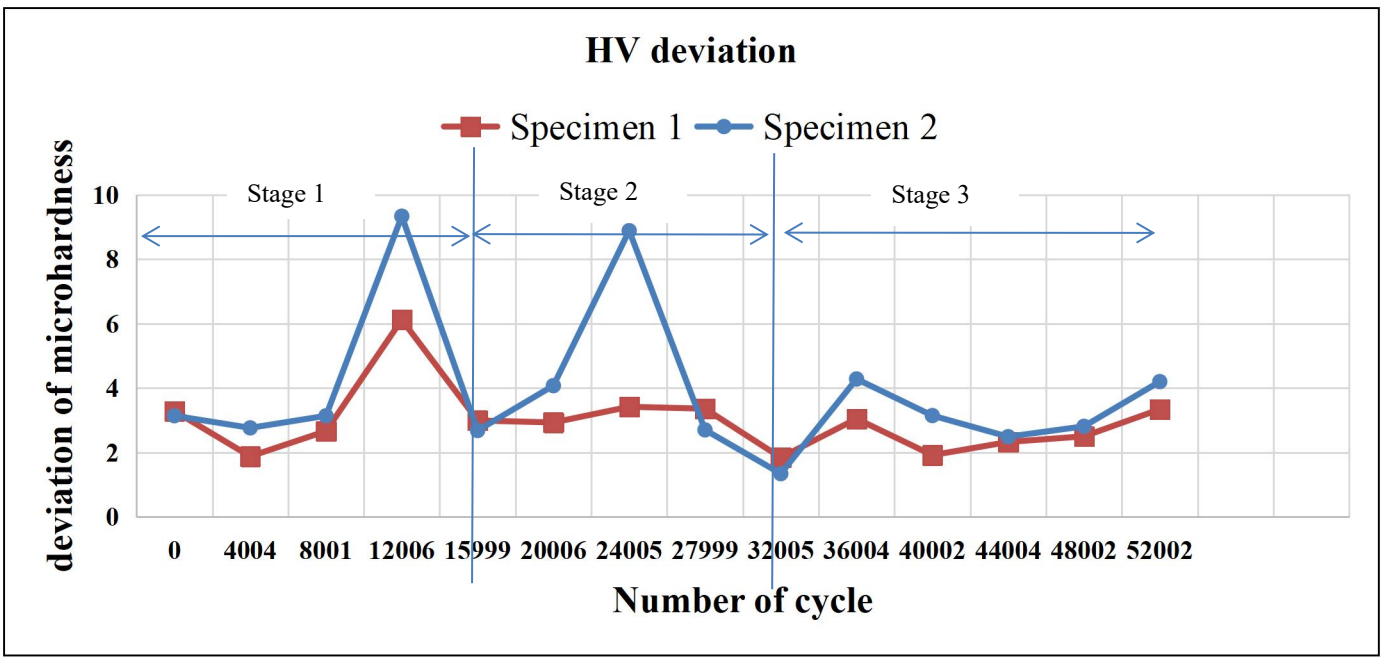

The figure 3.3 shows that the change of the average value of microhardness is very small, and it does not provide a good help for studying the microhardness change of the

material under the action of fatigue load. Therefore, the standard deviation of the microhardness is proposed, as shown in Figure 3.4.

From the figure 3.4, it can be found:

(1) For specimen 1, It can be found that the deviation of microhardness firstly decreases at the beginning, followed by two rapid increases and decreases, followed by a small increase and decrease, and finally shows an upward trend;

(2) For specimen 2, It can be found that the deviation of microhardness decreases at the beginning, followed by a rapid increase and decrease, followed by two small increases and decreases, and finally shows an upward trend;

(3) For both specimens, it was found that they have common characteristics: In the early stage of fatigue loading, its value first decreases, and then increases rapidly again with a rapid decrease. In the later stage of the fatigue load, there was a small increase and decrease, and finally showed an upward trend.

3.3. Discussion

From the part 1 we could find that the different materials have different behaviors under the cycling loads, even the same material with different internal structure, such as annealed C45 carbon steel and normalized C45 carbon steel.

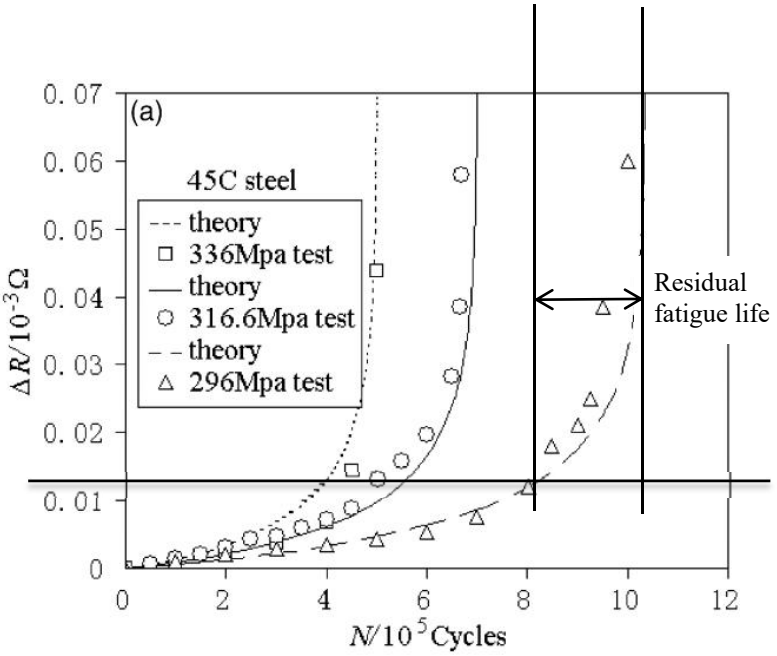

Figure 3.5 - Prediction of the C45 carbon steel residual fatigue life only used by electrical resistance testing [8].

According to Figure 1.10, the change in resistance of 45 carbon steel shows an exponential increase. This growth is also non-linear, but relatively simple. We can predict the residual fatigue life of material just by measuring resistance. As shown in Figure 3.5.

According to the research work of Geovana Drumond [27] and B. Pinheiro [7], it was also found that the experimental results by using microhardness testing and X-ray diffraction has the same three stages. As shown in Figure 3.6.

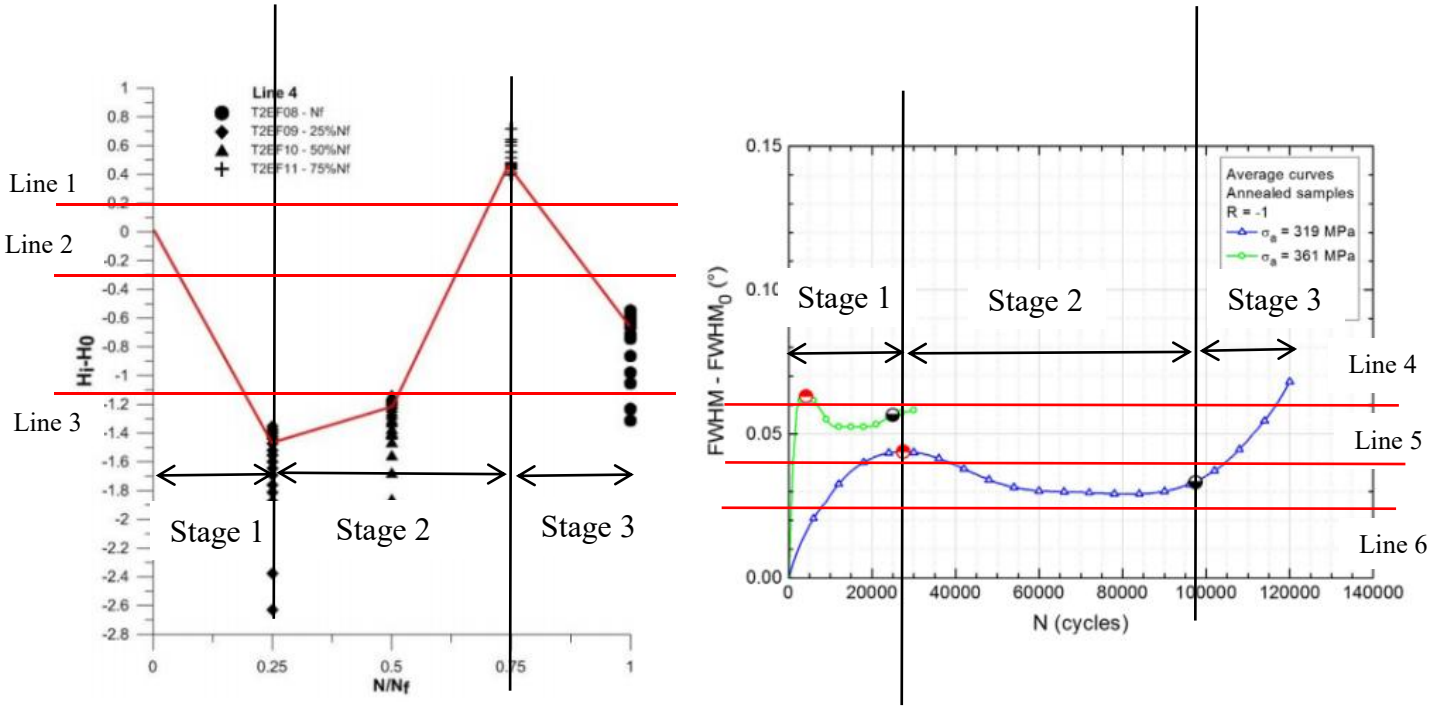

Figure 3.6 - Experimental results of API 5L X60 grade steel by using microhardness testing and X-ray diffraction [7,27].

From the figure 3.6, we can find that, the microhardness testing results have 3 possible positions:

(i) Line 1: the material may be in stage 2 or stage 3;

(ii) Line 2: the material may be in stage 1, 2 or stage 3;

(iii) Line 3: the material may be in stage 1 or stage 2.

As for X-ray diffraction, it also have 3 possible positions:

(i) Line 4: the material is in stage 3;

(ii) Line 5: the material may be in stage 1, 2 or stage 3;

(iii) Line 6: the material is in stage 1.

Combining the results of the two methods, it is possible to predict the residual fatigue life of materials.

Possible situations are:

(1) Line 1 + Line 4 = stage 3;

(2) Line 1 + Line 5 = stage 2 or stage 3;

(3) Line 2 + Line 4 = stage 3;

(4) Line 2 + Line 5 = stage 1, stage 2 or stage 3. Needing more testings to predict;

(5) Line 2 + Line 6 = stage 1;

(6) Line 3 + Line 5 = stage 1 or stage 2;

(7) Line 3 + Line 6 = stage 1.

So when there are more complicated nonlinear behaviour than the results shown in the Figure 3.5, it is more efficient and accurate to use two or more NDT methods to predict the residual fatigue life.

Conclusion to part 3

The TWIST loading spectrum was used in the fatigue testing in this work.

The microhardness testing of two D16T specimens shows the behaviour of deviation of microhardness could be divided into 3 stages during fatigue loading. It was found that two specimens have common characteristics: In the stage 1, deviation of microhardness firstly decreases, and then increases rapidly again with a rapid decrease. In the stage 3, there was a small increase and decrease, and finally showed an upward trend. However, in the stage 2, there is a big difference between two specimens. This may be caused by experimental error. To find out the exact behavior of the material, more experiments will have to be done.

For more complicated nonlinear behaviour of materials during cycling loading, it is more efficient and accurate to use two or more NDT methods to predict the residual fatigue life.

4. LABOR PROTECTION

Labor protection aims to promote a good working condition, focusing on wages, working hours and occupational safety and health (OSH) in terms of staff's economy, time and health. Labor protection measures mainly include legal, economic, social, technical and organizational aspects.

With the continuous improvement of laws and regulations and the promulgation of the Labor Protection Law, improving labor protection and working conditions, protecting workers' rights have become important issues of social concern. This work is based on theoretical researches and experimental testings. The workplace is located in the laboratory of National Aviation University. This work mainly requires fatigue tests and microhardness tests, and requires the operation of experimental machines Servo Hydraulic BiSS fatigue test machine, PMT-3M microhardness tester. This chapter will consider the laboratory's safe operating practices and the operator's labor protection.

4.1. Analysis of workplace conditions

According to the 2014 Hygienic standards "Hygienic classification of labor according to indicators of harmfulness and danger factors of the production environment, difficulty and tension of the labor process"[28]. Labor conditions are divided into four levels according to working environment, labor intensity, labor intensity and risk:

1. Class 1 (Optimum working conditions) - not only protects the health of employees, but also creates conditions for maintaining a high level of work capacity. Optimal hygiene standards are established for indicators of microclimate and labor process difficulty. This type of working conditions are generally considered optimal, in which case the adverse factors of the production environment do not exceed safe levels;

2. Class 2 (Acceptable Working Conditions) - Factors of the production environment and work process do not exceed established hygienic standard conditions (the functional state of the body may recover during the prescribed rest period or before the start of work), and should not be used against recent employees and their descendants adversely affect health;

3. Class 3 (harmful working conditions) - The hazardous production factors exceed specified hygiene standards and may harmfully affect the health of workers or their descendants. And this condition is divided into 4 categories based on the degree to which hygiene standards are exceeded and the severity of the possible harmful to the employee's body;

4. Class 4 (dangerous working conditions) - in this type of conditions, the harmful agents in the production environment and work process will pose a serious threat to the life of an employee, and has a high risk of acute occupational disease injury.

As for this work, all researches and experimental testings are achieved in the laboratory of National Aviation University, as shown in the figure 4.1. For the area of the laboratory is approximately $40m^2$ and volume of the workplace is 120 m^3. The laboratory consists of Servo Hydraulic BiSS fatigue test machine, PMT-3M microhardness tester, fire test chambers, computers and fire extinguishing devices.

Figure 4.1 - Schematic diagram of the laboratory.

4.2. Characteristics of dangerous and harmful factors

In order to improve working conditions that adversely affect potential workers, it is necessary to understand the harmful and dangerous factors present at work. Hazardous production factors are factors that may, under certain conditions, cause workers to become ill or continue to decline in their ability to work. Hazardous production factors are important factors that, under certain conditions, can lead to worker trauma or other sudden and dramatic health deterioration.

According to the ГОСТ 12.0.003-74 [29], Hazardous and harmful production factors are divided according to the nature of the action into the following 4 groups:
(i) physical; (ii) chemical; (iii) biological; (iv) psycho-physiological.

The possible hazardous and harmful production factors that could be appeared in the laboratory are:

(1) Microclimate (temperature, humidity);

(2) ionizing radiation;

(3) Concentration of pollutants (dust, CO2, benzene, acetone, etc.);

(4) Noise levels in the workplace;

(5) Vibration level;

(6) Electrical current;

(7) Lack of natural light;

(8) Insufficient lighting in the work area;

(9) Sharp edges and burrs on the surface of workpieces, tools and equipment;

In this works, the fatigue testings and microhardness testings are complicated are achieved at laboratory, considering that the instruments used in the laboratory for this work are Servo Hydraulic BiSS fatigue test machine and PMT-3M microhardness tester. The main hazardous and harmful production factors considered in this part are noise, electric shock and lighting limitations.

4.2.1. Noise

The main source of this work is fatigue testing. During fatigue testing, the machine generates noise due to cyclic loading.

Noise at work can cause permanent and disabling hearing damage. This can be gradual, with exposure to noise over time, but it can also be disrupted by sudden, very loud noises. Impairment is disabled because it prevents people from understanding language, having a conversation, or using the phone.

Hearing loss isn't the only problem. People may experience tinnitus, a distressing condition that can cause sleep disturbance.

Noise at work can interfere with worker communication, making warnings harder to hear. At the same time, it will also make people feel irritable and reduce safety awareness. These can lead to a safety risk of personal injury or death.

Employers must to carry out the several measures to reduce the influence of noise to the workers if any of the following situation appears:

- If the staff member needs to carry on a conversation at a distance of 2 meters;
- If workers need to use noisy tools or machines for more than half an hour a day;
- If the working condition is known to be under the influence of noise.

The results of measurements SPL in Octave Frequency Bands of laboratory are shown in the table 4.1.

Table 4.1 - Results of measurements SPL in Octave Frequency Bands of laboratory.

	Octave frequencies,Hz								L_Σ	L_A
	63	125	250	500	1000	2000	4000	8000		
$L_i(f)$	74	67	59	53	50	47	43	41	75	57.7

The total sound pressure level is calculated by the formula (6):

$$L_\varepsilon = 10\lg\sum_{i=1}^{i=8}10^{0.1Li} = 10\lg(10^{0.1\times74}+10^{0.1\times67}+10^{0.1\times59}+10^{0.1\times53}+10^{0.1\times50}+10^{0.1\times47}+10^{0.1\times43}+10^{0.1\times41}$$
$$\approx 75(\text{dB}) \quad (6)$$

And the noise level are calculated by formula (7):

$$L_A = 10\lg\sum_{i=1}^{i=8} 10(L_i - \Delta L_i) = 10\lg(10^{0.1\times(74-26.2)} + 10^{0.1\times(67-16.1)} + 10^{0.1\times(59-8.6)} + 10^{0.1\times(53-3.2)}$$
$$+10^{0.1\times(50-0)} + 10^{0.1\times(47+1.2)} + 10^{0.1\times(43+1)} + 10^{0.1\times(41-1.1)})$$
$$\approx 57.7(dB) \quad (7)$$

According to the Ukraine DCH 3.3.6.037-99 [30], the admissible sound pressure levels in Octave frequency bands are shown in the table 4.2.

Table 4.2 - The admissible sound pressure levels in Octave frequency bands [30].

Type of labour activity	Sound pressure levels in db in octave strips frequencies, Hz									L_A,dB
	31.5	63	125	250	500	1000	2000	4000	8000	
1. Creative activity	86	71	61	54	49	45	42	40	38	50
2. Highly skilled work	93	79	70	63	58	55	52	50	49	60
3. Work with acoustic signals	93	79	70	63	58	55	52	50	49	60
4. The work demanding a concentration	103	91	83	77	73	70	68	66	64	75
5. All other kinds of work, except point 1-4	107	95	87	82	78	75	73	71	69	80

4.2.2. electric shock

Due to the need for fatigue testing and microhardness testing in the laboratory, a lot of electrical equipment is required, and electric shock from accidental contact with the power source should be considered. The human body has good electrical conductivity, which means that electricity can easily pass through the body. Direct contact with electrical current can be fatal. While some electrical burns may appear small, there can still be serious internal injuries, especially to the heart, muscles, or brain.

The main hazards of electricity current are:

- Electricity affects the heart, causing cardiac arrest;
- Electric shock and burns due to contact with live equipment;
- Injury from contact with arcing, fire caused by faulty instrument or device;

- Thermal scald caused by contact with power source;
- Injured by falling after being electrocuted.

4.2.3. Lighting limitations

From a worker's perspective, lack of light at work can lead to eye strain, brain strain, headaches and accidents. On the other hand, too much light can also cause safety and health problems, such as glare and stress. Both can lead to work mistakes, poor quality and low productivity. Various studies have shown that good lighting in the workplace can increase productivity and reduce errors. For example, in the ILO manual [31]. The minimum and average lighting intensities required for different types of work are shown in the Table 4.3.

Table 4.3 -The minimum and average lighting intensities required for different types of work [31].

Activity	Typical Location	Average Illuminance (lux)	Minimum Illuminance (lux)
Movement of people, machines and vehicles.	Lorry park, corridors, circulation routes.	20	5
Movement of people, machines and vehicles in hazardous areas; rough work not requiring any perception of detail.	Construction site clearance, excavation and soil work, loading bays, bottling and canning plants.	50	20
Work requiring limited perception of detail.	Kitchens, factories assembling large components, potteries	100	50
Work requiring perception of detail.	Offices, sheet metal work, book binding.	200	100
Work requiring perception of fine detail.	Drawing offices, factories assembling electronic components, textile production.	500	200

4.3. Measures to reduce the impact of harmful and dangerous production factors

(1) Measures to reduce noise. There are many ways to reduce noise. The following practical measures can be taken to control noise risks:

- Use quieter equipment or different, quieter work processes;
- Reduce machine or working process noise at the source through engineering or technical controls;
- Use screens, barriers, walls and soundproofing materials to reduce noise transmission to exposed persons;
- Design and furnish workplaces for quiet workstations;
- Limit people's time in noisy areas.

(2) As for the measures to obtain sufficient lighting. It should be known that improvements in lighting don't necessarily mean installing more lights and using more electricity. Lighting levels can be improved by:

- Better use of existing lighting;
- Make sure all lights are clean and in good condition;
- Make sure there are lights where they are needed;
- Make the most of natural light.

(3) The following are measures to reduce electric injuries

- Install fuses, circuit breakers, or other devices to ensure that power is cut off in the event of a short circuit, reducing the chance of an accident due to a short circuit;
- Cables, plugs, sockets and accessories must be sufficiently strong;
- It must be ensured that the machine has an accessible switch or isolator to quickly cut off the power supply in an emergency;
- Regular inspection and testing of fixed wiring installations;
- ensure that anyone who needs to use electrical equipment has adequate skills, knowledge and experience;
- Make sure there are no trailing cables that could cause a person to trip or fall;
- Post electrical hazard or any other hazard signs.

4.4. Fire safety rules at the Laboratory

Three conditions are required to start a fire - a source of ignition, a source of combustible material and oxygen. In this work, ignition sources include heaters, lighting, open flames, electrical equipment, smoker's materials (cigarettes, matches, etc.), and anything else that can become very hot or cause sparks; fuel sources include wood, paper, Plastic, rubber or foam, loose packaging, trash and furniture; the source of oxygen and the surrounding air.

(1) In order to reduce the probability of fire, we can start from the source of fire and the source of combustible material.

The fire sources that may cause fires in the laboratory include short circuits or overheating of computers, cigarettes and matches, etc., and the combustibles that may cause fires include wood, paper, plastic, rubber and computers. Therefore, in order to reduce the probability of fire, it is necessary to strictly pay attention to the use of fire sources such as cigarettes and matches, and to regularly check the state of laboratory electrical equipment to prevent short circuits. At the same time, it is necessary to prevent the accumulation of combustibles in places where fire may occur.

(2) Measures to reduce injury in the event of a fire.

When a fire occurs, there needs to be some measures to reduce the probability of injury, such as using fire extinguishers, fire monitoring detectors, etc. In addition, it is necessary to know the escape routes of the laboratory, so that everyone can escape to safety as soon as possible in the event of a fire.

According to the DSTU EN 2: 2014 «Fire Classification» [32], the fires are divided into 4 classes: Class A – fires involving solid materials such as wood, paper or textiles. Class B – fires involving flammable liquids such as petrol, diesel or oils. Class C – fires involving gases. Class D – fires involving metals.

The main burning object in the laboratory is the computer, so the fire types are A-level and D-level. Therefore, the laboratory should be equipped with dry powder fire extinguishers and carbon dioxide fire extinguishers. And the placement of the fire extinguisher must be obvious and easily accessible. Fire extinguisher cabinets should not

be locked and require periodic inspection by laboratory personnel to prevent the extinguisher from being too low to operate.

In addition, the laboratory should post a schematic diagram of the emergency escape route (figure 4.2), and at the same time, the escape route guidance signs or indicators with fluorescent lights should be posted on the escape route floor.

The figure 4.2 - The schematic diagram of laboratory escape route.

Conclusion to part 4

This chapter mainly introduces the labor protection related issues of the laboratory used in this work. The harmful risk factors of laboratory staff are analyzed, and measures to improve the lighting, noise, electric shock and other elements of the working environment are proposed to ensure the safe operation of the laboratory and the health of the staff. At the same time, it also evaluates and analyzes the potential fire risk in the laboratory, considers the cause of the fire and proposes measures to reduce the probability of fire, and proposes measures to reduce the probability of casualties due to fire, such as installing fire extinguishers, fire detectors and usage of emergency escape routes.

5. ENVIRONMENTAL PROTECTION

5.1. The specifics of the impact of aviation transport on the environment

Transportation is an important contributor to national economic growth and an important driving factor for world economic growth. Air transport plays an important role globally, and in the last century it has grown to be the fastest, safest and most impactful mode of transportation. Today, more than 3 billion people use global air services. While aircraft carry only 0.5% of the world's traded goods, they account for 35% of international trade traffic, and achieving this result consumes only 2.2% of the world's energy used for transport. Aviation not only improves the quality of human life, effectively shortens the time required to visit relatives and friends, travel, etc., but also provides about 50 million jobs worldwide.

With the continuous expansion of the economy and the global population, the air transport industry has a bright future. However, as the impact of air transport on the environment continues to expand, it must be realized that the development of the air transport industry must be environmentally sustainable and the pollution to the environment must be reduced.

Air transport affects the environment in many ways: people near airports are affected by noise from aircraft; rivers can be affected by pollutants from airport rainwater; aircraft engines emit greenhouse gases and pollutants into the atmosphere.

5.1.1. Climate change

The widespread use of fossil fuels in the air transport industry has resulted in a large increase in aircraft emissions, noise, and particulate matter, drawing global attention to the impact of air transport emissions on local air quality [33]. Jet airliners emit greenhouse gases such as carbon dioxide and small amounts of nitrogen oxides, wakes and particulate matter through the combustion of fuel in their engines. As shown in the figure 5.1, in 2018, the global air transport industry was estimated to be responsible for 2.4% of global anthropogenic CO_2 emissions [34].

Although the fuel efficiency of jet airliner engines has improved by 70% over the past four decades, and CO_2 emissions per kilometer in 2018 were 47% of 1990 levels, but overall emissions increasing year by year duo to the increase of air transport. By 2020, air transport emissions will be 70% higher than in 2005 and may increase by 300% by 2050 [35].

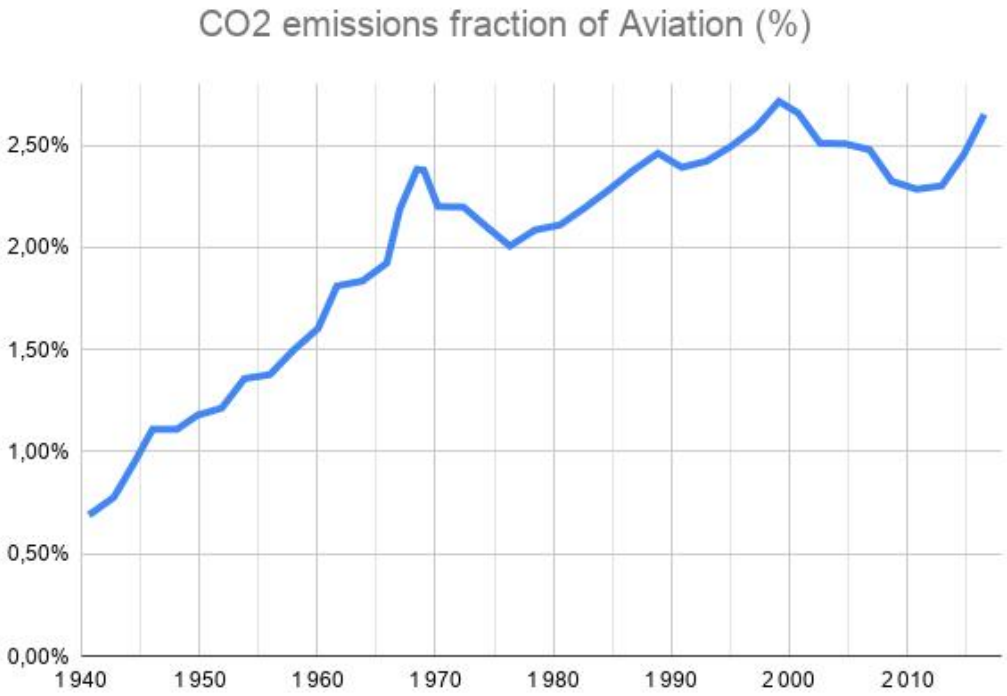

Figure 5.1 - The increasing of CO_2 emissions fraction of aviation between 1940 to 2018.

Aircraft engine emissions are more than 90% of aircraft engine exhaust is oxygen and nitrogen in the normal atmosphere, and others are mainly carbon dioxide, water, nitrogen oxides, carbon monoxide incompletely burned fuel, sulfide and carbon, which are roughly the same composition as car exhaust. Although the main greenhouse gas emitted by jet aircraft is carbon dioxide, it is fundamentally different from the ground because jet airliners emit the gas mainly when they fly in the troposphere. Airplanes affect climate in four ways as they fly in the troposphere:

- Carbon dioxide: Carbon dioxide emissions are the most important part of the air transport industry gas emissions. In addition to the CO_2 emissions from aircraft engines, the airport ground handling vehicles, vehicles used by passengers to travel to

the airport, airport construction and aircraft manufacturing also contributes to the CO_2 emissions;

- Nitrogen oxides: At the troposphere, nitrogen oxides emitted by aircraft contribute to the formation of ozone (O_3) in the troposphere. Also, nitrogen oxides emitted in the troposphere have a greater impact on ozone formation than those emitted at the ground level, resulting in higher concentrations of ozone in the atmosphere at an altitude of 10 kilometers, which in turn has a greater global warming effect;
- Contrails and cirrus clouds: Fuel combustion produces water vapor that condenses into a white trail at high altitudes or in cold conditions. Although trails emit lower emissions than carbon dioxide, they are also considered one of the culprits of the global greenhouse effect. Cirrus clouds form after persistent wakes have formed, and studies have shown that they also contribute to an additional global warming effect;
- Particulates: Compared to emissions such as carbon dioxide, sulfate and carbon dust particles have a smaller direct impact on the environment. But they can affect the quality of the air and thus human health. And when soot particles are large enough, they are thought to cause the most contrails to form.

5.1.2. Noise

Aircraft noise has been a concern since inception of ICAO , but it is limited to the noise produced when the propeller tip is spinning at nearly the speed of sound. However, with the introduction of jet aircraft around the world in the last century, people have gradually become aware of the impact of the noise produced by jet aircraft on the surrounding environment. Because aircraft noise intensity is proportional to engine power. So reducing power reduces noise, but at the same time may affect the safety features of the jet.

In 1968, the ICAO Assembly adopted a resolution discussing the serious effects of aircraft noise on the environment near airports and instructing the ICAO Council to develop international norms and related guidance material to control aircraft noise levels near airports. In 1971, the General Assembly passed another resolution discussing the possible adverse effects of aircraft activity on the environment. The resolution proposes

responsibilities of ICAO to protect the global environment and benefit the people of the world, as well as to promote the compatibility between the healthy and orderly development of civil aviation and the human living environment.

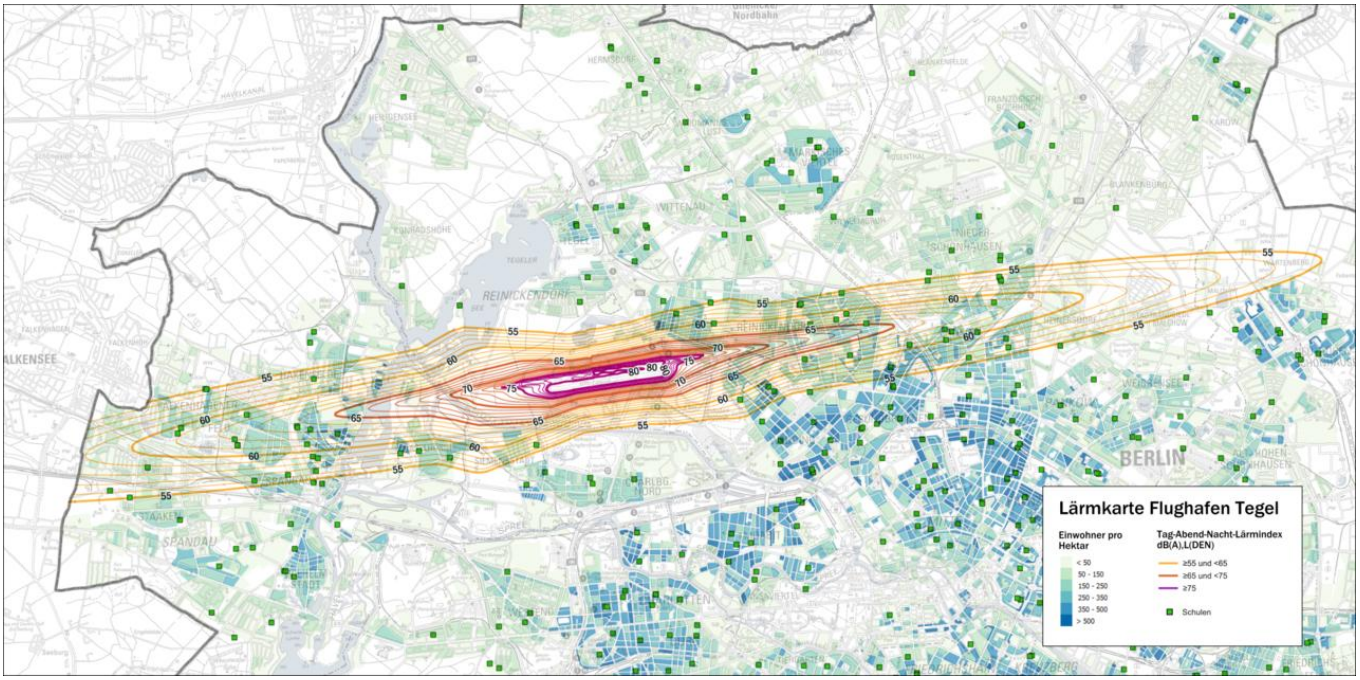

Figure 5.2 - Noise around the Berlin Tegel Airport.

5.1.3. Water pollution

Due to the long-term and extensive use of fossil fuels, lubricants and other chemicals, leaks are inevitable, resulting in serious water pollution on the airport grounds.

Including de-icing fluids used in cold weather, where de-icing fluids contain ethylene glycol or propylene glycol, since most of them fall to the ground, they will flow with the water to nearby streams, rivers or coastal waters, as shown in the figure 5.3. Since ethylene glycol and propylene glycol consume oxygen in the water during the degradation process, the oxygen content of the water is reduced, and ultimately the death of aquatic organisms is caused.

In addition, road de-ice are used on airport runways and taxiways, which contain potassium acetate, glycol compounds, sodium acetate, urea and other chemicals that also affect the environment around the airport.

Figure 5.3 - Excess aircraft deicing fluid may contaminate nearby water bodies.

5.1.4. Air pollution

Ozone is a substance that can seriously affect respiratory health hazards. According to statistics, 6,800 people die prematurely each year due to ozone, and the main anthropogenic source of ozone is air transportation [36]. In addition, aircraft engines emit ultrafine particles in and near airports during takeoff and landing, as do ground handling equipment. During takeoff, it was measured that about 3 to 50 x 10^{15} particles per kilogram of fuel burned.

According to the survey, in the United States, more than half of the private jet piston engines released lead into the air from burning Avgas, resulting in the release of approximately 34,000 tons of lead into the atmosphere over the past 40 years. And the United States Federal Aviation Administration research found that inhaled or ingested small amounts of lead can adversely affect the nervous system, red blood cells, cardiovascular and immune systems. Exposure to lead-containing air in infants and young children may cause behavioral and learning problems and lead to mental decline.

5.1.5. Aircraft waste

Due to its cheap and easy-to-use properties, plastics are widely used in aircraft cabins, such as tableware provided for passengers, so a large amount of garbage is generated, as shown in the figure 5.4. According to the latest statistics from the International Air Transport Association (IATA), in 2017, each passenger generated an average of 1kg of waste per flight, and the total passenger waste was 6 million tons. Most of these are paper, cardboard, and plastic, among others. But as air transport grows and more and more people fly, the amount of waste generated will only increase.

Figure 5.4 - waste in the aircraft.

In addition, when the aircraft is retired or scrapped in an accident, it will also face the problem of generating waste. When aircraft are retired, they are dismantled(figure 5.5), and most of the metal is recycled. However, there are also some difficult-to-recycle materials in aircraft, such as glass, textiles, plastics, etc. Some of these difficult-to-recycle garbage will be incinerated, and some will be buried, which will pollute the environment.

Figure 5.5 - dismantling of the aircraft.

5.2. Measures for environmental protection

(1) Measures taken by ICAO:

The International Civil Aviation Organization (ICAO) is an agency established by the United Nations in 1947 under the Convention on International Civil Aviation. Currently, ICAO has 193 member states and is responsible for the governance and regulation of global civil aviation affairs. Its purpose is to provide principles and technologies for global navigation, to promote the norms of international air transport, and to ensure the efficient operation of international civil aviation. The 19 Annexes promulgated by ICAO list the Standards and Recommended Practices (SARPs) expected by States signatories to ICAO Conventions. They elaborate on the Standards and Recommended Practices and provide insight into what signatories must do and how to achieve them. Among them, Annex 16 - Environmental Protection was developed to regulate the impact of aviation on the environment.

Annex 16 provides SARPS for the environmental protection of the global air transport industry, making a great contribution to reducing the impact of air transport on the environment. Annex 16 deals primarily with the protection of the environment from aircraft noise and aircraft emissions – two topics that were barely considered when the

Chicago Convention was signed. In general, Annex 16 on environmental protection has 4 volumes, as follows:

(i) Volume I - Aircraft Noise;

(ii) Volume II - Aircraft Engine Emissions;

(iii) Volume III - Aircraft CO2 Emissions;

(iv) Volume IV - Carbon Offsetting and Reduction Scheme for International Aviation (CORSIA).

ICAO promotes international cooperation in these areas by developing new global aviation standards. In addition, ICAO Member States discussed and formulated goals for international aviation and proposed prioritizing environmental protection resources in the following areas:

- Innovations in airframes, engines and other aircraft components and technologies;
- Optimize flight procedures to reduce fuel consumption;
- Increase the use and development of sustainable aviation fuels and clean energy;
- Implement the Carbon Offsetting and Reduction Scheme for International Aviation (CORSIA).

(2) Reducing air travel:

- Route optimization: Emissions can be effectively reduced by improving air traffic management systems, developing more direct routes and optimizing cycle altitudes. For example, in 1999 the European Union proposed a single European sky plan to avoid overlapping airspace restrictions between EU countries and reduce emissions [37]. Until today, the plan has not been fully implemented, resulting in the emission of more than 10 million tons of carbon dioxide;
- Emissions trading: ICAO approved measures to reduce CO_2 emissions from air transport through emissions trading, which limiting CO_2 emissions from airlines through the implementation of an emissions trading scheme, while providing incentives for airlines to develop more efficient technologies to reduce emissions;
- Short-haul ban: The short-haul ban is a government measure that prohibits airlines from establishing and maintaining short-haul routes, in order to reduce the number of

air flights and thus lessen the impact on the environment. Forcing people to use public transport with a lower environmental impact, such as trains, when travelling short distances.

(3) Taxes and subsidies:

By increasing aviation taxes, people can be motivated to consider other cheaper and more environmentally friendly travel options. And increasing airline subsidies can encourage airlines to innovate in technology to improve fuel efficiency.

(4) Use of alternative fuels:

- Biofuels: Aviation biofuel is a type of biofuel used to power aircraft and, unlike traditional fossil fuels, is a sustainable aviation fuel. Biofuels are derived from plant or waste biomass, which can be extracted from jatropha, algae, animal fats, etc. The biggest advantage of sustainable biofuels is that they are sustainable and they do not compete with crops and forests. Compared to conventional fossil fuels, they can reduce CO_2 emissions by 20% to 90% depending on the biomass source [38]. And in 2019, the International Transport Association set a target of 2% biofuel use in total fuel by 2025;
- Hydrogen and e-fuel: In 2020, Airbus introduced a liquid hydrogen-powered zero-emission aircraft concept and is preparing to launch a prototype in 2035 [39]. According to the research report, the emission reduction cost of hydrogen-based electronic fuel is about 1,000 euros per ton of carbon dioxide. By 2050, the cost could fall to about 100 euros per ton of CO_2, but it may not be enough to replace fossil fuels. Therefore, hydrogen-based electronic fuel technology still has a long way to go from maturity to application.

(5) Electric aircraft:

Electric aircraft use renewable electricity and operate without any emissions. Take lithium-ion batteries, for example, which are about 30 times more efficient at converting energy than fossil fuels. In 2020, the first electric aircraft was certified, however it is

estimated that the electric aircraft that may be successfully researched in this century are small pure electric aircraft (currently developed and certified), large hybrid aircraft. And large long-haul aircraft are unlikely to be electrified within this century.

Although pure electric aircraft has been proven to be achievable, it is uncertain whether the aircraft can be completely converted from traditional fuel to electricity. And from the perspective of current battery technology, the currently commonly used lithium batteries have the shortcomings of short battery life and fragile and easy to catch fire, and their battery capacity will decrease with the increase of use time. Therefore, alternatives to lithium batteries, such as the recently developed sodium batteries, are currently being sought.

Conclusion to part 5

In this chapter, the specifics of the impact of aviation transport on the environment are discussed. And found the main impact on the environment are: climate change, noise, water pollution, air pollution and aircraft wastes. And the measures for environmental protection are also discussed, such as: measures taken by ICAO, reducing air travel, taxes and subsidies, use of alternative fuels and electric aircraft.

GENERAL CONCLUSION

Fatigue failure is a common failure mode of aircraft metals and alloys. Because of its inevitability and destructiveness, it has been widely studied. Subject of study is analyzing nonlinear behavior of material properties under cycling to predict residual fatigue life. And the aim of master degree thesis is to predict residual fatigue life of materials by using microhardness testing method.

In this diploma work, the following works have been completed:

1. The linear method to predict the residual fatigue life was discussed. And it was realized that linear method is not reliable, because of some elementary shortcomings: experimental data are scattered; stress amplitudes below the fatigue limit will not cause damage; ignores the residual stress effect at the notch;

2. The nonlinear methods to predict the residual fatigue life was discussed. And found that NDTs were widely used in crack detection and fatigue life prediction because it could detect defects, chemical and physical parameters using rays, ultrasound, infrared, electromagnetic and without destroying the properties of materials. The existing research works on studying the nonlinear behaviour of properties of materials by using NDT were analyzed, such as X-ray diffraction, electrical resistance testing, acoustic emission and microhardness testing. And compared these NDT methods, found the microhardness testing method is more simple and suitable to predict fatigue life;

3. Aluminum alloy Д16Т plates with a thickness of 1.24 mm, and a width of 0.4 mm were used to do fatigue testings and microhardness testings. In fatigue testing, servo hydraulic BiSS fatigue test machine was used, and main components of the machine were introduced. In microhardness testings, microhardness tester PMT-3M was used. The main components and experimental procedure to use of the machine were introduced;

4. In the fatigue testings, the TWIST loading spectrum was used, which was the most widely used load spectrum in fatigue studies of transport aircraft wings. And the main parameters of TWIST loading spectrum were introduced. And in fatigue testings, two specimens were used for a total of 52,002 cycles. The microhardness measurement interval is approximately 4000 cycles. In order to eliminate errors, a total of 10 microhardness

measurements were carried out in each interval, and the average value of the 10 measurement results was taken as the microhardness of this cycle;

5. The microhardness testings results shown that the microhardness change could divided into three stages. And for both specimens, it was found that they have common characteristics: In the first stage of fatigue loading, the value microhardness firstly decreases, and then increases rapidly again with a rapid decrease. In the third stage of the fatigue load, there was a small increase and decrease, and finally showed an upward trend. The only downside is that in the second stage, the results of two specimens shown a different trend, which may be caused by experimental error. To find out the exact behavior of the material, more experiments should be done;

6. By analyzing the resistance change of C45 carbon steel, and the research results of API 5L X60 stainless steel microhardness experiment and XRD experiment. It is proposed that when the nonlinear change of material properties under fatigue load is relatively simple, only one NDT technology can accurately predict fatigue life. When the performance changes are more complex, the use of a variety of non-destructive testing techniques can improve the accuracy of predicting fatigue life;

7. Labour protection related to the laboratory used in this work were discussed. The main harmful factors and fire safety rules at the Laboratory in the laboratory were introduced. And the measures to reduce the impact of harmful factors were also introduced. The specifics of the impact of aviation transport on the environment were discussed, and measures for environmental protection were also introduced.

In this work, microhardness tests of two D16T aluminum alloy specimens were carried out only, and the test results showed that the microhardness of aluminum alloys is a complex nonlinear change. It is difficult to predict its fatigue life from microhardness alone. Therefore, in the follow-up work, it is necessary to use other NDTs to conduct experimental research on D16T aluminum alloy to accurately predict its fatigue life.

REFERENCE

[1] S.K. Bhaumik, M. Sujata, M.A. Venkataswamy. Fatigue failure of aircraft components. Engineering Failure Analysis 15 (2008) p675–p694.

[2] A. May*, M.A. Belouchrani, A. Manaa , Y. Bouteghrine. Influence of fatigue damage on the mechanical behaviour of 2024-T3 aluminum alloy. Procedia Engineering 10 (2011) 798–806.

[3] J. Schijve. Fatigue of Structures and Materials. 2009. (Chapter 10, p295-p327)

[4] Schijve, J., Some remarks on the cumulative damage concept. Minutes 4th ICAF Conference, Zürich (1956) paper 2.

[5] Haibach, E., Modified linear damage accumulation hypothesis accounting for a decreasing fatigue strength during increasing fatigue damage (in German). Laboratorium für Betriebsfestigkeit, LBF, Darmstadt, TM Nr.50 (1970).

[6] G. Maeder, J.L. Lebrun, J.M. Sprauel. Present possibilities for the X-ray diffraction method of stress measurement. NDT Int. 14 (5) (1981) 235–247.

[7] B. Pinheiro, J. Lesage, I. Pasqualino, E. Bemporad, N. Benseddiq. X-ray diffraction study of microstructural changes during fatigue damage initiation in pipe steels: Role of the initial dislocation structure. Materials Science & Engineering A 580 (2013) 1–12.

[8] Binxiang Sun, Yimu Guo. High-cycle fatigue damage measurement based on electrical resistance change considering variable electrical resistivity and uneven damage. International Journal of Fatigue 26 (2004) 457–462

[9] Riccardo Nobile, Andrea Saponaro. Real-time monitoring of fatigue damage by electrical resistance change method. International Journal of Fatigue 151 (2021) 106404.

[10] R. Nobile, A. Saponaro. Electrical Resistance measurements for fatigue damage prediction of AISI 316L stainless steel. Procedia Structural Integrity 41 (2022) 421–429.

[11] Scruby, C. An introduction to acoustic emission. Journal of Physics E: Scientific Instruments 20 (2000) 946.

[12] Fredrik Bjørheim, Sudath C. Siriwardane, Dimitrios Pavlou. A review of fatigue damage detection and measurement techniques. International Journal of Fatigue 154 (2022) 106556.

[13] Roberts TM, Talebzadeh M. Acoustic emission monitoring of fatigue crack propagation. J Constr Steel Res 2003;59(6):695–712.
[14] Roberts TM, Talebzadeh M. Fatigue life prediction based on crack propagation and acoustic emission count rates. J Constr Steel Res 2003;59(6):679–94.
[15] Yu J, Ziehl P, Zrate B, Caicedo J. Prediction of fatigue crack growth in steel bridge components using acoustic emission. J Constr Steel Res 2011;67(8):1254–60.
[16] Keshtgar A, Modarres M. Acoustic emission-based fatigue crack growth prediction. Proceedings - Annual Reliability and Maintainability Symposium. 2013.
[17] Ye D., Wang Z. (2001). An approach to investigate pre-nucleation fatigue damage of cyclically loaded metals using Vickers microhardness tests. International journal of fatigue, 23(1), 85-91
[18] Duyi Ye, Xiaoyan Tong, Leijiang Yao, Xiaoxia Yin. Fatigue hardening/softening behaviour investigated through Vickers microhardness measurement during high-cycle fatigue. Materials Chemistry and Physics 56 (1998) 199-204.
[19] Du-Yi Ye, De-Jun Wang, Ping An. Characteristics of the change in the surface microhardness during high cycle fatigue damage. Materials Chemistry and Physics 44 (1996) 179-181.
[20] P. Heuler, H. Klatschke. Generation and use of standardised load spectra and load–time histories. International Journal of Fatigue 27 (2005) 974–990.
[21] De Jonge, J.B., Shutz, D., Lowak, H., Schijve, J., A Standardized Load Sequence for Flight Simulation Tests on Transport Aircraft Wing Structures, National Aerospace Laboratories Technical report NLR-TR 73029U, Amsterdam, 1973.
[22] Sunder, R, Contribution of individual spectrum load cycles to damage in notch root crack initiation, short and long crack growth, ASTM STP 1211, American Society for Testing and Materials, 1993, pp 19-29.
[23] R. Sunder. Fatigue Crack Growth under Flight Spectrum Loading with Superposed Fuselage Cabin Pressure. International Journal of Fatigue 33 (2011) 1101–1110.
[24] I Milne, RO Ritchie, BL Karihaloo. Comprehensive structural integrity Volume 4 - Cyclic loading and fatigue. 2003, books.

[25] Yajun CHEN, Ailun WANG, Fusheng WANG, Xianchao WANG. Fatigue Behaviors of 2024 Aluminum Alloy under Aviation Load Spectrum. Journal of Aeronautical Materials 2016 36(5): pp64-69.

[26] M. Brod, A. Dean, S. Scheffler, M. Bishara, R. Rolfes. Numerical Analysis of Fatigue Damage Behavior in Fiber Composites under Different Block Loading Conditions. 10.23967/composites.2021.024

[27] Geovana Drumond, Francine Roudet, I. Pasqualino, B. Pinheiro, Didier Chicot, Xavier Decoopman. High cycle fatigue damage evaluation of steel pipelines based on microhardness changes during cyclic loads. 2017.

[28] Гігієнічна класифікація праці за показниками шкідливості та небезпечності факторів виробничого середовища, важкості та напруженості трудового процесу : Державні санітарні норми та правила від 30.05.2014 р. № z0472-14. Редакція від: 30.05.2014.

[29] ГОСТ 12.0.003-74. Опасные и вредные производственные факторы. Классификация.

[30] ДСН 3.3.6.037-99 Державні санітарні норми виробничого шуму, ультразвуку та інфразвуку ДСН.

[31] Physical Hazards, indoor workplace lighting. https://www.ilo.org/wcmsp5/groups/public/@americas/@ro-lima/@sro-port_of_spain/documents/presentation/wcms_250198.pdf.

[32] Класифікація пожеж (EN 2:1992; EN 2:1992/A1:2004, IDT) [Текст] : ДСТУ EN 2:2014. – На заміну ГОСТ 27331-87; чинний з 01.01.2016 / Мінекономрозвитку України, 2014. – 7 с. (Державний Стандарт України).

[33] "Aircraft Engine Emissions". International Civil Aviation Organization.

[34] Brandon Graver; Kevin Zhang; Dan Rutherford (September 2019). "CO2 emissions from commercial aviation, 2018" . International Council on Clean Transportation.

[35] "Reducing emissions from aviation". Climate Action. European Commission. 23 November 2016.

[36] Eastham, Sebastian D.; Barrett, Steven R. H. (1 November 2016). "Aviation-attributable ozone as a driver for changes in mortality related to air quality and skin cancer". Atmospheric Environment. 144: pp17–23.
[37] Crespo, Daniel Calleja; de Leon, Pablo Mendes (2011). Achieving the Single European Sky: Goals and Challenges. Alphen aan de Rijn: Kluwer Law International. pp. 4–5.
[38] Bauen, Ausilio; Howes, Jo; Bertuccioli, Luca; Chudziak, Claire (August 2009). "Review of the potential for biofuels in aviation". CiteSeerX 10.1.1.170.8750.